PROCESSING AND INTERPRETATION OF ELECTROMAGNETIC INDUCTION ARRAY DATA

GARY D. EGBERT
College of Oceanic and Atmospheric Sciences, Oregon State University, Oregon, USA
E-mail: egbert@coas.oregonstate.edu

(Received 2 November 2000; Accepted 7 July 2001)

Abstract. The simultaneous nature of array data can be exploited in electromagnetic induction studies for three general purposes. First, one or more reference sites can be used to reduce bias, improve signal-to-noise ratios, and provide better control over source complications and coherent noise in estimates of MT impedances and other EM transfer functions (TFs). Although a single good reference site can dramatically improve TF estimates, improvements due to multiple sites are often rather modest, because local noise is the limiting factor. Secondly, arrays allow for estimation of inter-station transfer functions, and maps of anomalous horizontal field variations. Relatively straightforward modifications to inversion codes would allow quantitative interpretation of these additional constraints on resistivity variations. Finally, with arrays it is possible to estimate the response of the Earth to a richer spectrum of external source excitations. In particular, the natural extension to the usual uniform source assumption implicit in the MT method allows for three curl-free magnetic gradient sources. Quantitative interpretation of the response of a three-dimensional Earth to these sources could provide additional constraints on large scale variations in crustal and upper mantle resistivity, and might help to overcome problems due to aliasing of near surface distortion in widely spaced MT data.

Keywords: array data, Earth, electromagnetic, magnetometers MT arrays, MV arrays

1. Introduction

Two dimensional arrays of magnetometers have made valuable contributions to our understanding of both external magnetic variation fields, and the large scale pattern of electrical resistivity in the crust and upper mantle. Use of the magneto-variational (MV) approach by the induction community peaked in the late 1960's and 1970's, after development of low cost three component magnetic variometers (Gough and Reitzel, 1967). During this era a number of large two-dimensional arrays of widely spaced instruments (often hundreds of km apart) were deployed throughout the world. Reviews of these array experiments, with discussion of their contribution to our understanding of the the solid Earth are provided by Gough (1973), Frazer (1974), Gough (1983), Gough and Ingham (1983), Alabi (1983), and Gough (1989). The EMSLAB array (Gough et al. 1989; Figure 1) is an example of one of the largest of these arrays, which we will consider in some detail in our discussion. With the MV approach anomalous concentrations of currents are

Surveys in Geophysics **23:** 207–249, 2002.

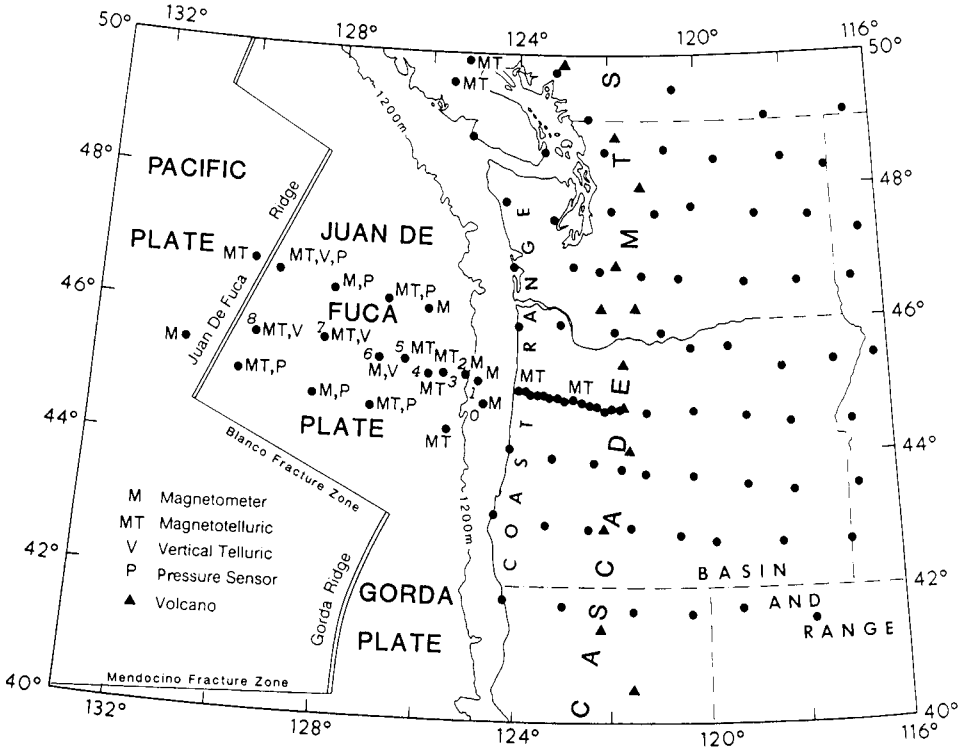

Figure 1. EMSLAB Juan de Fuca array (after Gough et al., 1989).

detected by reversals of the vertical component, and local enhancements of horizontal components, of the magnetic variation fields. Because the inversion of MV data for crustal and upper mantle resistivities is highly non-unique, Gough (1989) concluded that array studies were best used as a qualitative tool for mapping and discovery, with more detailed follow up magnetotelluric (MT) surveys necessary to image structures quantitatively.

Over the past 15 years the major advances in our understanding of large scale resistivity variations in the crust and upper mantle have come from interpretation of comparatively dense linear MT profiles across specific (generally elongated) features of interest (e.g., Wannamaker et al., 1989; Jones and Craven, 1990; Chen et al., 1997; Unsworth et al., 1997; Cerv et al., 1997; Fujinawa et al., 1997, among many others). The MT method is based on the ratio of the electric to magnetic fields at a single point. Thus, although interpretation of MT data in a two or three dimensional environment certainly requires observations at arrays of locations, these data need not be simultaneous. Transfer function methods allow "stacking" of data from a number of time windows to estimate a uniform source, or plane wave, impedance which is independent of time, and characteristic of only the location. For long period MT data logistical considerations often dictate simultaneous collection of

data at a small number of sites, but interpretation of this data ultimately does not directly depend on simultaneity of the observations. Indeed, MT profiles are often built up over a number of field seasons.

Single site approaches have also frequently been used for long period geomagnetic depth sounding (GDS), where an equivalent 1-d MT impedance is computed as a ratio of local magnetic field components (e.g., Schultz and Larsen, 1987; Bahr and Filloux, 1989). All of these single site methods require assumptions about the nature of external sources. For the case of MT, sources must be quasi-uniform (i.e., varying slowly over length scales exceeding the skin depth (Dmitriev and Berdichevsky, 1979)). This assumption is relatively weak, and holds reasonably well except perhaps at high latitudes and long periods (e.g., Garcia et al., 1997). For the GDS approach lateral gradients of the magnetic fields are used in place of electric fields, and to compute these from data at a single site very strong assumptions are required about both the external sources and the underlying resistivity distribution. In this case assumptions are much stronger, and only hold under some conditions (e.g., simplified models for Sq such as used by Bahr and Filloux (1989) may be workable on true solar quiet days for periods of one day and a few harmonics; the P_1^0 source assumption holds for periods beyond about 5 days at mid-latitudes (Banks, 1969; Schultz and Larsen, 1987)).

Although single site measurements have proven to be quite effective for EM induction studies of crustal and mantle electrical structure, there are a number of potential advantages to array approaches. Most obviously, arrays provide direct constraints on the spatial structure of external sources. This was of course a major motivation for deployment of two-dimensional arrays some three decades ago when mapping of geomagnetic variations on the Earth's surface (e.g., Bannister and Gough, 1978) was still the best way to gain an understanding of ionospheric and magnetospheric current sources. Although satellite observations now provide more detailed *in situ* observations, magnetometer arrays continue to be useful for studies of external magnetic variation sources (e.g., Chi and Russell, 1998). Through better understanding of these sources we can improve processing and interpretation of data for induction studies. Arrays may also be useful for understanding and ameliorating the effects of cultural noise on MT soundings (e.g., Larsen et al., 1996, Egbert, 1997; Ritter et al., 1998), and for reducing the effect of incoherent noise (Egbert, 1997). In addition to providing better control over possible source effects on local EM TFs, arrays can be used to map anomalous concentrations of currents resulting from laterally heterogeneous resistivity. This can be accomplished directly through single event maps or magnetogram stacks (e.g., Gough and Ingham, 1983), or indirectly through inter-station TFs (e.g., Beamish and Banks, 1983; Egbert and Booker, 1993). Simultaneous observations thus provide new interpretation parameters. Fitting these with a formal inversion procedure, along with more traditional single site parameters such as MT impedances and vertical field TFs, can enhance resolution of some features. Finally, arrays allow interpretation of a richer spatial spectrum of external sources. GDS methods rely on strong as-

sumptions about the spatial structure of external sources. With an array of large enough size spatial gradients of the magnetic fields can be directly estimated (e.g., Jones, 1980; Olsen, 1998), reducing the need to rely on *a priori* assumptions.

Advances in instrumentation have made deployment of large arrays of fully digital MT systems feasible. The recent Baltic Electromagnetic Array Research (BEAR) experiment (Korja et al., 2000) with 50 full MT systems, and an additional 20 permanent magnetic variometers covering the Fennoscandian shield (Figure 2), provides a good example of the sort of large scale experiment that can now be conducted. With all data digital and electric fields measured along with magnetic variations, this array represents a significant advance relative to the large MV arrays of the past. More generally, multi-channel wide-band MT data sets (with arrays of several tens of dipoles and/or multiple remote sites) are now commonly acquired during routine applied surveys. Given these developments, a review of methods for processing and interpreting data from arrays of EM instruments seems appropriate at this time. Rather than providing a comprehensive review of either array experiments that have recently been completed, or of all methods that have been proposed that make use of multiple sites, I provide an overview of some of the important issues. As readers will discover, the overview is very much from the perspective of the author, and I emphasize examples from my own work with arrays in the Western US to illustrate the discussion. These include the EMSLAB array, other three component MV arrays from the same area in the Northwestern US (Egbert and Booker, 1993), and some small MT arrays from near the San Andreas Fault south of San Francisco, California (Figure 3). Obviously most of the same points could be made with examples from a large number of other arrays from around the globe.

The focus throughout is on induction applications of arrays. Applications of arrays to studies of source characteristics are not considered except insofar as they impact induction studies. The paper is organized around the three general uses of array data outlined above. First, in Section 2, I consider uses of array data to improve estimates of local transfer functions such as MT impedances. I include in this discussion remote reference processing which uses a very small (possibly only two site) array, as well as methods based on larger arrays with multiple sites. In Section 3, I consider uses of arrays to extend the usual local-site plane wave TFs to include inter-station TFs, and hypothetical event analysis. Finally, in Section 4, I consider how arrays can allow us to exploit induction by a richer spatial spectrum of external sources for mapping resistivity variations in the Earth. This last area is certainly the least developed, and possibly the most important. Large scale MT arrays (e.g., the BEAR array of Figure 2) have stations spaced so widely that aliasing of near surface features (which can distort MT data to arbitrarily long periods) might be expected to result in significant depth uncertainties at even the largest scales. New and more sophisticated processing and interpretation methods for arrays may help to reduce this uncertainty, since multi-dimensional gradient methods based on magnetic fields will not be distorted by near surface features in

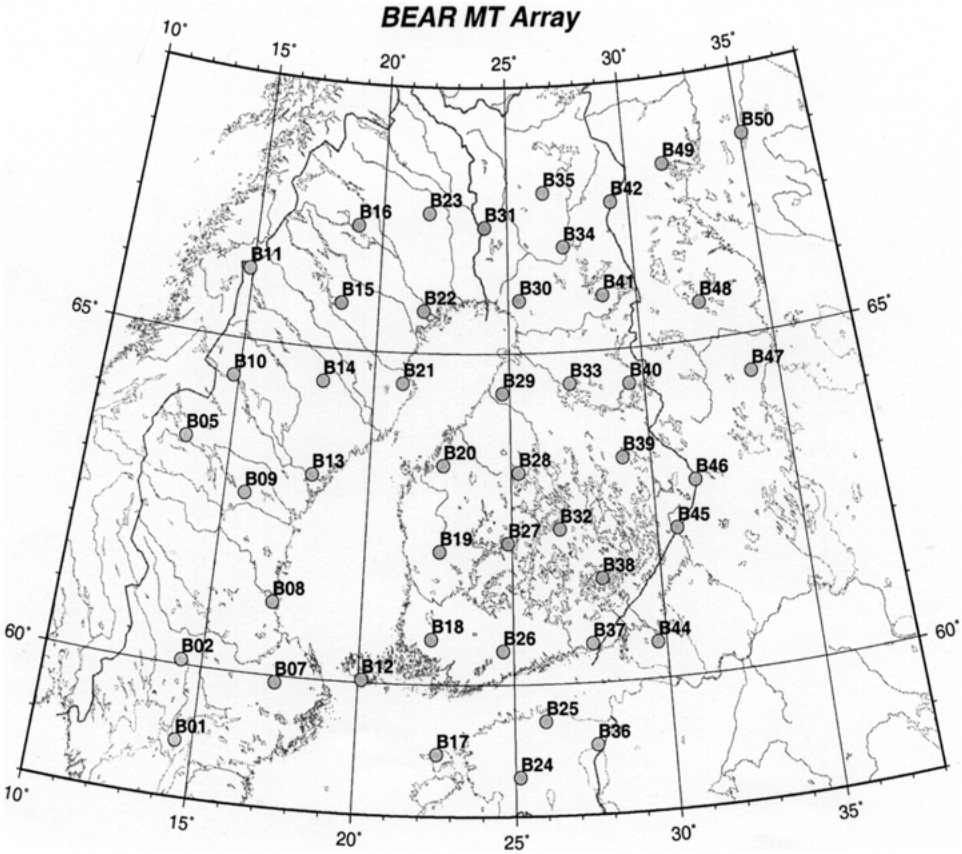

Figure 2. Baltic Electromagnetic Array Research (BEAR) MT and magnetometer array (BEAR Working Group, personal communication, 2001).

the same way that the electric components are. In this last section the focus will be on ideas for future developments, rather than a review of previous publications.

2. Multi-site Processing for Local TFs

2.1. Remote reference

Making the usual MT assumption that the external sources are spatially uniform, and allowing for noise in the simplest way, electric and magnetic field components at a single site are related in the frequency domain through a 2×2 transfer function (TF)

$$\mathbf{e} = \mathbf{Z}\mathbf{h} + \epsilon, \tag{1}$$

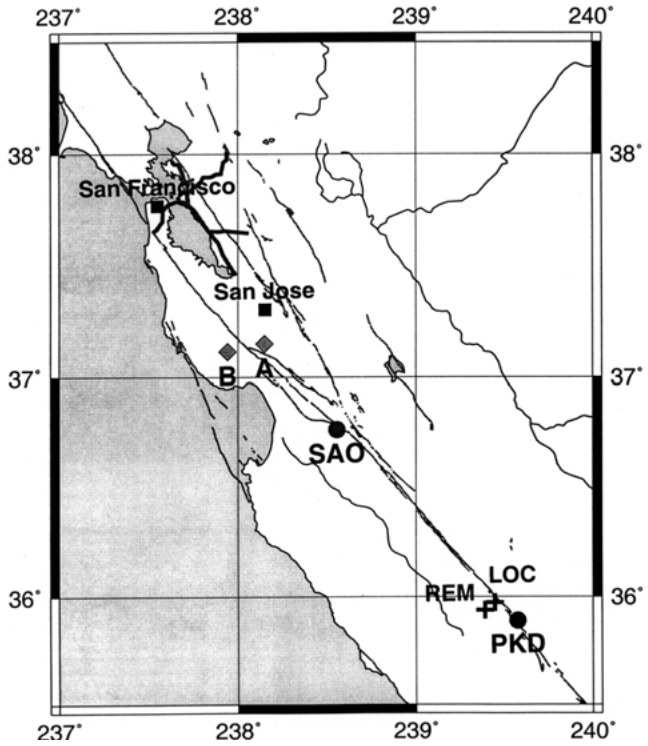

Figure 3. Location map for three small (two-site) MT arrays south of San Francisco, California. Filled circles: UC Berkeley SAO/PKD monitoring array (Egbert et al., 2000). Shaded diamonds: local (A) and remote (B) sites from a MT survey near the site of the 1989 Ms 7.1 Loma Prieta earthquake (Mackie and Madden, 1992). Crosses northeast of PKD: nearby local and remote sites from an MT profile across the San Andreas Fault (Unsworth et al., 2000).

where ϵ represents noise. In the MT case the TF $\mathbf{Z}$ is generally referred to as the impedance tensor. However (1), and all of the following discussion of estimation, hold equally well for the case of vertical field and interstation TFs, so we use this generic term TF in the following discussion. The frequency dependent TF $\mathbf{Z}(\omega)$ can be estimated quite simply by Fourier transforming the time series, and using linear least squares (LS) to minimize the misfit to (1) over a series of time segments (and/or nearby frequencies). The estimate can be written

$$\hat{\mathbf{Z}} = \left\langle \mathbf{e}\mathbf{h}^* \right\rangle \left\langle \mathbf{h}\mathbf{h}^* \right\rangle^{-1}, \tag{2}$$

where the brackets denote averages, and the superscript asterisk the conjugate transpose. It was recognized long ago (e.g., Sims et al., 1971) that noise in the predicting $\mathbf{h}$ channels would cause an over-estimate of the magnitude of the magnetic field auto-power (the diagonal of $\left\langle \mathbf{h}\mathbf{h}^* \right\rangle$), and hence a downward bias of impedance amplitudes. Figure 4a gives an example of the sort of bias that is often seen in MT data at periods of around 1–10 s or so, for a site near Parkfield, California (the

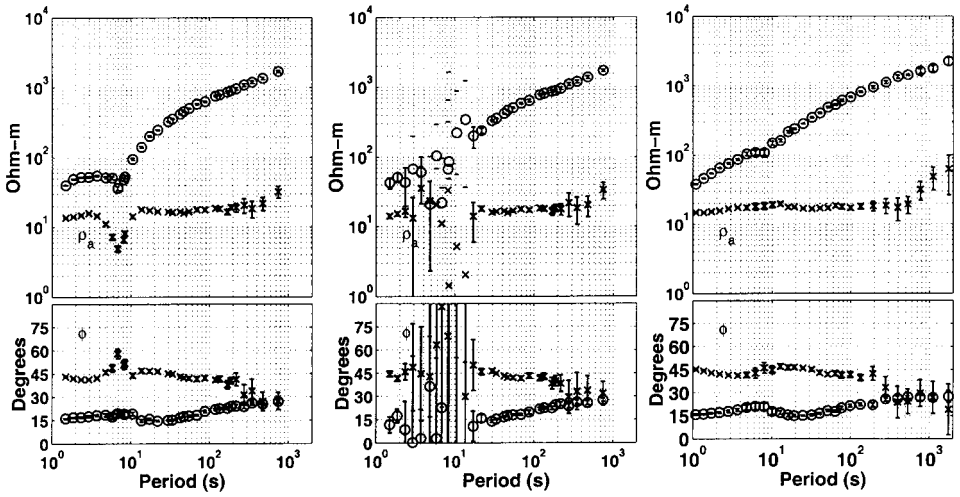

Figure 4. Single site and remote reference TE and TM mode MT apparent resistivities and phases for a site near Parkfield, California (crosses in Figure 3). (a) Single site estimates, showing a sharp bias in amplitude and phase at a period of around 7 seconds. (b) Robust remote reference estimates are severely degraded by noise in the remote channels. (c) Processing the same data set with an alternative robust remote reference scheme, which also allows for outliers at the remote site (Egbert, 1997), significantly improves parameter estimates.

crosses in Figure 3). To avoid these bias errors the remote reference (RR) method was developed (Gamble et al., 1979a). For RR, horizontal magnetic fields $\mathbf{r}$ are recorded simultaneously at a second (remote) site and cross-correlated with the EM fields at the local site:

$$\hat{\mathbf{Z}} = \langle \mathbf{e}\mathbf{r}^* \rangle \langle \mathbf{h}\mathbf{r}^* \rangle^{-1} . \tag{3}$$

The RR method is one of simplest, yet most useful, ways in which simultaneous MT data at multiple sites can be used to improve the quality of local TF estimates. The basic idea is almost trivial, but nonetheless very important: with more than one site it is much easier to distinguish between noise and the coherent signal that we want to interpret.

In many cases neither the natural source signal, nor the dominant noise sources, are well modeled as stationary Gaussian processes, causing LS type approaches (including the standard RR estimate (3)) to fail catastrophically. To allow for outliers the regression M-estimate (RME; e.g., Huber, 1981) was adapted to MT TF estimation by Egbert and Booker (1986) and Chave et al. (1987). Chave and Thomson (1989) proposed a straightforward extension of the RME to the RR case. Equation (3) is replaced by a weighted version

$$\hat{\mathbf{Z}} = \langle w\mathbf{e}\mathbf{r}^* \rangle \langle w\mathbf{h}\mathbf{r}^* \rangle^{-1} . \tag{4}$$

with weights for individual segments $w = w(\mathbf{e} - \hat{\mathbf{Z}}\mathbf{h})$ determined adaptively from the misfit between electric and magnetic components at the local site. The estimate is iterative, with small weights assigned to poorly fitting data (as determined using the impedance estimate from the previous iteration). This procedure is generally initialized using a standard (LS) RR estimate. One problem with this formulation of the robust RR estimator is that it does not explicitly allow for outliers in the remote site channels **r**. As illustrated in Figure 4b outliers in the remote can seriously degrade TF estimates, so for a truly robust RR estimate it is necessary to also identify and downweight outliers in **r**. One simple approach is to simultaneously estimate transfer functions between **h** and **r**, and make data weights for the RR estimate of the impedance depend also on the misfit between local and remote components (Egbert, 1997). An example of the effectiveness of this approach is given in Figure 4c.

2.2. MULTIVARIATE PROCESSING

EM array data are highly multivariate, with multiple components recorded simultaneously at multiple stations, but even the RR estimate is based on an essentially univariate statistical procedure. Egbert and Booker (1989) described a general theoretical framework for processing data from arrays of simultaneously recording EM instruments based on classical methods of multivariate statistical analysis. Egbert (1997) combined the multivariate approach with the RME to develop a practical robust multivariate errors-in-variables (RMEV) estimator for small (2–10 station) arrays of MT instruments. With the RMEV approach data from all channels are used to improve signal-to-noise ratios, and to diagnose possible biases due to coherent noise. The possibility of noise, and outliers, in all data channels is allowed for explicitly. The RMEV approach thus provides a natural (though not the only) solution to the problem with outliers in the remote channels seen in Figure 4.

As the multivariate perspective will be useful for discussion of many aspects of EM array data, it is worthwhile to review some basic ideas and terminology here. To be explicit we assume initially that there are 5 channels of data at each of J stations, for a total of $K = 5J$ channels in the array. Generalization to other cases is straightforward. Allowing for noise in all channels, the frequency domain MT array data vectors $\mathbf{X}_i$ for a fixed frequency band satisfy:

$$\mathbf{X}_i = \begin{pmatrix} \mathbf{h}_{1i} \\ \mathbf{e}_{1i} \\ \vdots \\ \mathbf{h}_{Ji} \\ \mathbf{e}_{Ji} \end{pmatrix} = \sum_{m=1}^{M} \mathbf{u}_m \alpha_{mi} + \sum_{l=1}^{L} \mathbf{v}_l \beta_{li} + \epsilon \tag{5}$$

$$= [\mathbf{u}_1 \ \ldots \ \mathbf{u}_M]\,\mathbf{a}_i + [\mathbf{v}_1 \ \ldots \ \mathbf{v}_L]\,\mathbf{b}_i + \epsilon = \mathbf{U}\mathbf{a}_i + \mathbf{V}\mathbf{b}_i + \epsilon, \tag{6}$$

where $i = 1, \ldots, I$ index the time segments. The K dimensional vectors $\mathbf{u}_m$, $m = 1, M$ are the signal vectors, i.e., the components of magnetic fields at the J

measurement sites that are consistent with our prior source assumptions. In the terminology of Egbert and Booker (1989), these signal vectors span the response space. For the usual quasi-uniform source assumption of the MT method $M = 2$ and $\mathbf{u}_1, \mathbf{u}_2$ give the total fields associated with two independent source polarizations (e.g., spatially uniform linearly polarized N-S and E-W sources, which we denote as $\mathbf{u}_x$ and $\mathbf{u}_y$ respectively). The time varying parameters α_{mi} define the particular linear superposition of sources observed in any event (e.g., the polarization of uniform magnetic sources for the standard two component MT case). The remaining terms on the right side of (5) define the noise model, including L sources of coherent noise (with generalized noise "polarization" parameters $\beta_{li}, l = 1, L$), and a K dimensional incoherent noise vector ϵ, with diagonal error covariance $\Sigma_N = \mathbf{E}(\epsilon\epsilon^*)$.

The model of Equation (5) is completely general, and is especially useful for exploratory analysis of signal and coherent noise characteristics. The first step in the multivariate processing procedure is to estimate the variance, or scale, of incoherent noise in each data channel (i.e., the elements of the diagonal matrix Σ_N). This is accomplished by fitting each channel to the remaining data channels, and computing residual variances. Egbert (1997) describes a robust, approximately unbiased variant on this simple idea, which allows for noise and outliers in all data channels. The second step is to estimate the "coherence dimension" of the array data, i.e., the total number of independent coherent signal and noise vectors $N = M + L$. This is accomplished by computing the eigenvector decomposition of the scaled spectral density matrix (SDM), the $K \times K$ matrix of all possible component cross-product averages $\mathbf{S} = \langle \mathbf{X}\mathbf{X}^* \rangle = 1/I \sum \mathbf{X}_i \mathbf{X}_i^*$:

$$\mathbf{S}' = \Sigma_N^{-\frac{1}{2}} \mathbf{S} \Sigma_N^{-\frac{1}{2}} = \mathbf{W}\Lambda\mathbf{W}^*. \tag{7}$$

In (7) $\Lambda = \mathbf{diag}(\lambda_1, \ldots \lambda_K)$ is the diagonal matrix of eigenvalues and $\mathbf{W}$ the orthonormal matrix whose columns are the corresponding eigenvectors. If the full signal can be explained in terms of only plane wave MT sources and incoherent noise (the assumption implicit in all standard TF estimation schemes), there should be only two eigenvalues of $\mathbf{S}'$ significantly larger than one (Egbert, 1997). More generally, in the presence of coherent noise or more complex sources the number of significant eigenvalues N will exceed two.

An example of eigenvalue spectra as a function of period is given for a two station MT array in Figure 5. The two MT sites in this array, denoted SAO and PKD in Figure 3, have operated almost continuously since 1996 at two sites near the San Andreas Fault in central California (Egbert et al., 2000; Eisel and Egbert, 2001). For periods from about 10–300 s the coherence dimension of the array exceeds 2, indicating that there is coherent noise ($L > 0$) and/or that the external source magnetic fields cannot be completely characterized by the two parameter plane wave model. In this particular case, Egbert et al. (2000) show that the additional coherent degrees of freedom in the array observations arise primarily from very

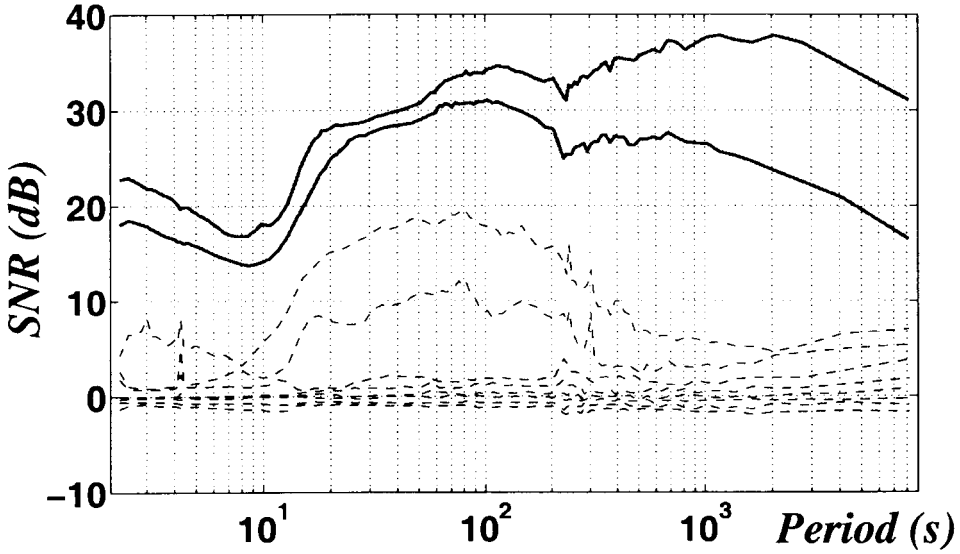

Figure 5. Spectrum of normalized eigenvalues of the 10 × 10 cross product matrix (SDM) for the SAO/PKD MT array (filled circles in Figure 3; after Egbert et al., 2000). Each data channel is normalized by an estimate of the incoherent noise amplitude, so eigenvalues are non-dimensional and give signal-to-noise ratios of coherent sources. For ideal uniform source MT data there should be only two eigenvalues significantly above the background (zero dB) incoherent noise level. For periods 10–300 s two additional independent sources are required to characterize the spatially coherent data (so N = 4). Egbert et al. (2000) show that these additional sources can be explained by spatial complexity in the Pc3 band near T = 15 s, and coherent noise due to DC electric trains in the San Francisco Bay area 150–300 km to the north.

large scale cultural noise from a DC electric commuter railway in the San Francisco Bay area far to the north (the so-called BART system; see Figure 3). However, near a period of 15 s the very small spatial scale of Pc3 pulsations (e.g., Chen and Hasegawa, 1974; Waters et al., 1991) also complicates the array signal.

The eigenvectors associated with the N significant eigenvalues provide an estimate of the space spanned by the columns of the signal and coherent noise matrices **U** and **V**. However, without some additional information it will not generally be possible to uniquely separate **U** from **V** (Egbert, 1997). If we find that the number of eigenvalues above background noise levels is two, the array data are consistent with plane wave sources with no coherent noise. In this case the two eigenvectors associated with the two significant eigenvalues provide an estimate of **U** (more strictly, of the span of the columns of **U**). MT impedances and all other sorts of single site and inter-station uniform source TFs are readily computed from this matrix (Egbert and Booker, 1989).

As with the RR estimate, the RMEV is not biased by noise in the input channels. In fact, the multiple station estimate can be viewed as a remote reference scheme, with the reference signal **r** defined as an optimal linear combination of all data channels (Egbert, 1997). By using all data channels to estimate the reference signal,

estimation variances for single station TFs can be reduced. However, RR estimates of TFs are degraded by noise in all of **h**, **e**, and **r**. By using many sites we can effectively reduce noise in the reference fields **r**, but these extra sites do not directly do anything to reduce noise in the local electric and magnetic channels **h**, **e**. As a result only modest improvements in estimator performance are typically achieved by using multiple sites in processing.

The multivariate approach does provide a very natural way to allow for outliers in all channels, and as we shall discuss further subsequently, it provides a natural framework for exploratory analysis of signal and coherent noise characteristics in EM array data. As illustrated in Egbert (1997) insights gained from this sort of analysis can lead to significant improvements in TF estimates in noisy environments.

2.3. USE OF MULTIPLE REMOTE SITES

Varentsov et al. (2001) have proposed a simpler way to take advantage of multiple remote sites in a large array. Separate robust remote reference estimates of local TFs are computed using a number of remote sites at different distances and azimuths from the local site. These are then averaged using a robust procedure. Experiments with the BEAR MT sites suggests that at least some improvement in impedance estimates is achieved by averaging results obtained with from 3 to 10 separate remote sites (Figure 6).

Comments made about the multivariate approach are also relevant here. Averaging a number of TF estimates might seem to offer the possibility of significant reductions in estimation errors. However, all of the estimates must use the same local electric and magnetic fields, and so do not have independent estimation errors. Again, by using multiple remotes we can reduce noise in the reference **r**, but will still be limited by noise in **h** and **e**. However, as with the multiple station method there may be other more subtle advantages to computing and robustly averaging TF estimates with several remote sites in a large array, as the results of Figure 6 suggest.

2.4. SOURCE DIAGNOSTICS AND COHERENT NOISE

Since array data provide some information about the actual source fields, both coherent noise and complications in the geometry of natural sources can be much more easily diagnosed than with single site data. For example, in the BEAR array it is possible to directly map polar ionospheric current systems (Viljanen et al., 2000). Sokolova et al. (2001) showed that biases in MT impedances tended to be largest when polar current systems were most intense. Information about source complexity determined from the array can thus be used to select data with the best source characteristics for MT processing. However, if even a single remote site is separated from the local site by many skin depths, remote reference processing might be expected to already eliminate serious source biases in MT impedances, since

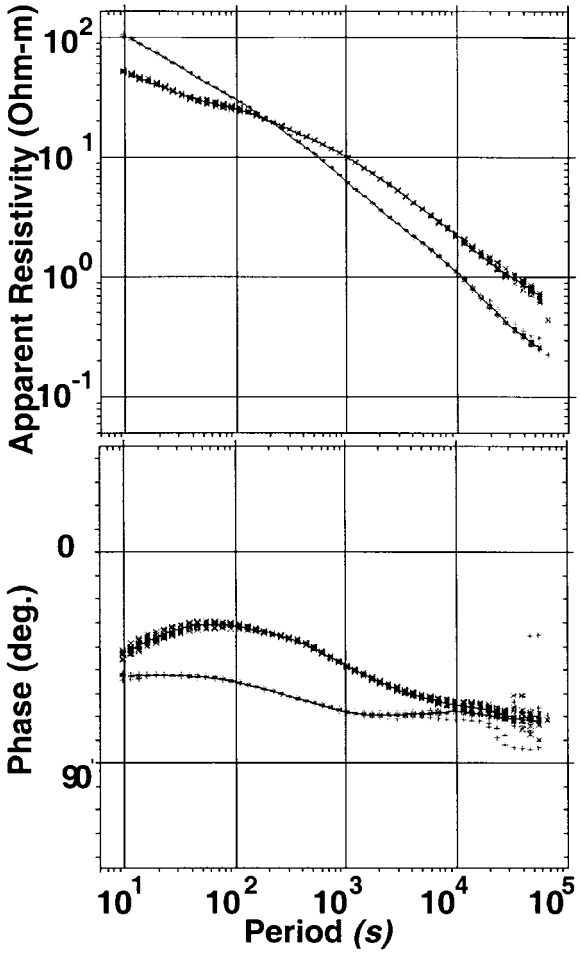

Figure 6. Remote reference estimates of apparent resistivity and phase for site B02 in the BEAR array (Figure 2), processed as described in Varentsov et al. (2001). The cloud of symbols give estimates obtained using 9 different remote sites; the line gives results of a robust average of all RR estimates.

source fields with wavelengths short enough to cause bias would not generally be coherent between such distant sites. Indeed, for the BEAR MT data Sokolova et al. (2001) found that the robust remote reference scheme used by Varentsov (2001; see also Ernst et al., 2001), which rejected data sections that showed either low coherence (between **e** and **h**, or between magnetic fields at local and remote sites), tended to already eliminate data segments with the worst source characteristics (Figure 7). At least in this case even single station coherence criteria appear to be effective at eliminating data contaminated by local polar source current systems.

Simple robust RR processing may be less effective for vertical field TFs at lower frequencies, or for inter-station TFs with large site separations. For both of these cases systematic effects due to the finite spatial scale of sources will be

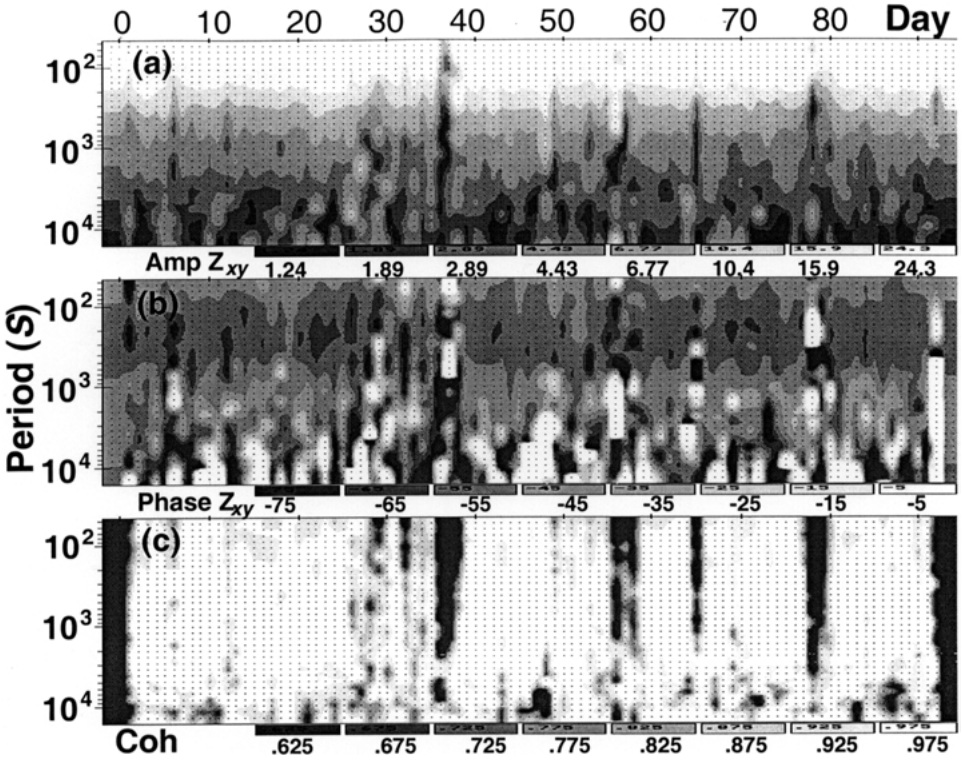

Figure 7. (a) Amplitude and (b) phase of the impedance element Z_{xy} from site B11 in the BEAR array (Figure 2), as a function of period and day during the three month deployment. Multiple coherence between E_x and the two local horizontal magnetic components (c), is reduced during the times when amplitude and phase are most erratic. Sokolova et al. (2001) show that data from these low coherence segments correspond to source complications due to nearby polar ionospheric current systems. Eliminating this data improves stability and accuracy of the impedance estimates.

more severe, and selecting data segments based on array source diagnostics can offer more significant advantages. For example, for an array of 29 sites under the equatorial electrojet in Brazil, Arora et al. (1998) found from examination of simultaneous time series that sources had much larger spatial scales in the evening hours. Inter-station vertical field TFs estimated from night-time data were found to be significantly less affected by the short spatial scales associated with the electrojet, and thus more indicative of internal structure.

RR is also less effective at eliminating coherent noise when arrays are of small spatial extent. Egbert (1997) considered the problem of data selection in a very small array consisting of two MT sites separated by approximately 20 km. The sites, denoted A and B in Figure 3, were about 50 km south of the San Francisco Bay Area, significantly closer to the source of coherent BART train noise than the two station SAO/PKD MT array. At this distance the train noise had significant power in spatial scales short enough to cause bias in the impedances, but still large

enough to be coherent over the 20 km separating the local and remote sites. As a result there were significant biases in even RR estimates (Figure 8a). Egbert (1997) discussed multivariate array diagnostics which could be used to look for time windows with minimal coherent noise contamination. All were based on projecting the array data into the N-dimensional space defined by the significant eigenvectors computed from the full data set, and then calculating diagnostics in short time windows using the projected data. Examples include eigenvalues of the SDM, and interpretation parameters computed from the first two eigenvectors (Figure 9). In this case there was a clear time window of about 2 hours duration where all diagnostics indicated that coherent noise problems were minimal (Figure 9). Selecting only this data led to significant improvements in MT impedance estimates (Figure 8b). The success of this particular data selection exercise appears to be strongly dependent on the rather sharp temporal division between "bad" and "good" data (later understood to result from the nightly shutdown of the BART train system). Other efforts to apply these sort of time domain diagnostics to MT data sets from Bavaria with more continuous coherent noise problems have not been as successful (M. Eisel, personal communication 1999). Clearly the best solution to problems of coherent noise is to maintain one or more remote sites a number of skin depths distant from the local sites. One true remote is almost certainly more useful for cancellation of coherent noise than a large array of nearby sites.

A different approach to the problem of coherent noise in small arrays has been proposed by Larsen et al. (1996). These authors also worked with MT data contaminated by coherent DC electric train noise, this time in Italy. If both the "train noise" and uniform source signals were directly observed, a generalized four component TF could be estimated relating the electric fields to both sets of magnetic field sources. It is readily verified that an unbiased uniform source MT impedance would then be recovered from the appropriate part of the four input TF. Including the magnetic fields due to the train in the prediction would reduce noise and improve TF estimates. Since it isn't possible to actually measure either the train noise or the local uniform source magnetic fields by themselves, Larsen et al. (1996) suggest using uncontaminated remote channels ($\mathbf{r}$) from a distant site to estimate the natural source magnetic fields $\hat{\mathbf{h}}_{MT}$ at the local site (via an interstation TF), and the residuals from this fit $\hat{\mathbf{h}}_{Train} = \mathbf{h} - \hat{\mathbf{h}}_{MT}$ as a surrogate for the train noise. In fact, as the authors point out, for standard least squares processing this two-source scheme reduces exactly to the usual remote reference method. For the non-linear robust estimates, where data weights are computed adaptively, the equivalence between the two-source scheme and a more conventional robust RR is no longer exact, and different results will be obtained with the two approaches. One possible advantage of the two-source scheme is that all of the predictable signal (due to both MT and train sources) can be used to identify and clean up incoherent noise. The multiple station method of Egbert (1997) also takes advantage of this possibility, by using both MT and coherent noise sources for initial damping of incoherent noise. However, there is no obvious reason for the two-source scheme

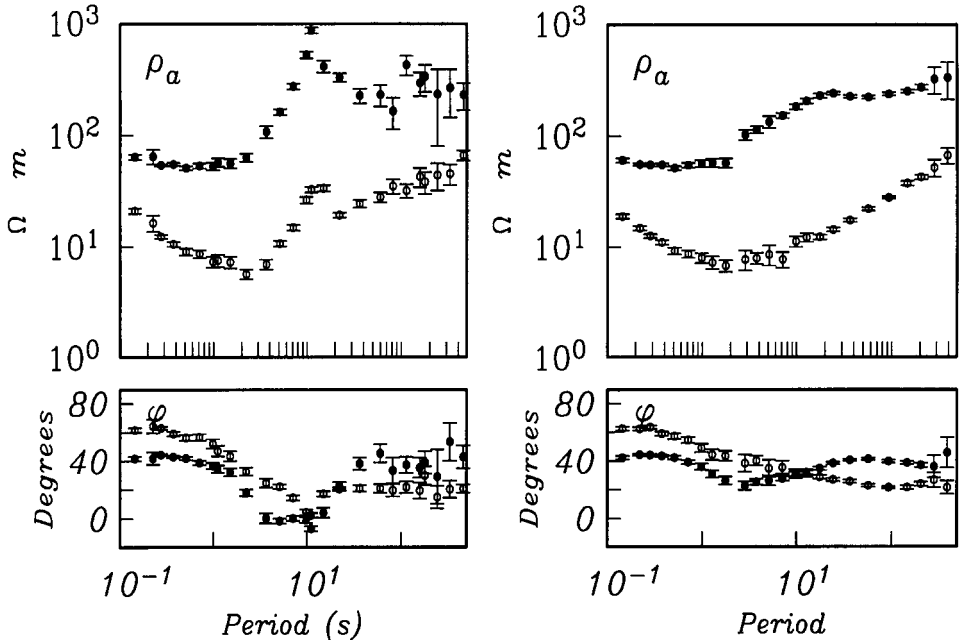

Figure 8. Remote reference MT apparent resistivity and phase estimates from a site near the 1989 Ms 7.1 Loma Prieta earthquake (site A in Figure 3; site B was used the remote). In (a) all data were processed with a robust RR procedure, allowing for outliers in all channels. Significant biases are evident near a period of 10 s. For (b) the array coherent noise diagnostics of Figure 9 were used to select a subset of data for processing (i.e., data for hours 0–2), leading to much better results. After Egbert (1997).

to be more effective in ameliorating the effects of coherent noise than a careful application of more standard robust RR methods. The fundamental requirement in all cases – RR, multiple station, or Larsen's two-source approach – is a true remote site, unaffected by noise that is coherent with the local site.

3. Anomalous Horizontal Fields

3.1. Event maps

MT impedances and vertical field TFs are normalized by the total (internal plus external) local magnetic field. Lateral variations of resistivity redistribute and concentrate currents, so that even with completely uniform sources, there will be lateral variations in the horizontal magnetic fields, which can be directly mapped with large arrays. These maps are especially effective for detecting narrow elongated conductive anomalies (Gough, 1989). Gough and Ingham (1983) review techniques for mapping and interpreting anomalous internal currents with the large arrays of analogue recording magnetic variometers deployed to that time. The simplest

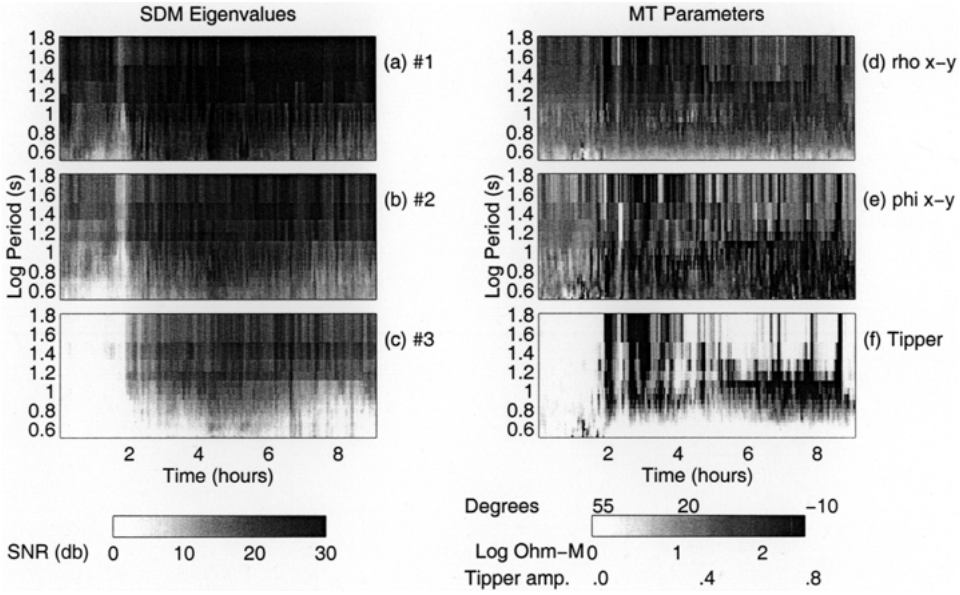

Figure 9. Coherent noise diagnostics computed for the two station array A/B of Figure 3 (after Egbert, 1997). Diagnostics were constructed by first computing an eigenvector decomposition of the full data set, projecting the data into the space spanned by the three dominant eigenvectors, and then computing various quantities for a series of short time windows. In (a–c) the three largest eigenvalues of the SDM are plotted. Before hour 2 there are only two eigenvalues significantly above normal background incoherent noise levels. During this time window estimates of apparent resistivities, phases, and vertical field TFs are also much better behaved. Note in particular the tendency for the vertical field TF amplitudes to increase greatly and become erratic after hour 2.

approach is to contour components of the magnetic variations interpolated from the observation sites for one or more fixed times. With modern computer technology it is of course quite straightforward to extend this idea to make a movie of the time evolution of the interpolated magnetic fields. Although these simple time domain images provide only qualitative information about Earth resistivity, they may offer significant insight into the nature of the source fields.

A slightly more effective (and quantitative) approach is to first Fourier transform data for a single "event" or time window, and then contour amplitude and phase (or real and imaginary parts) of the Fourier coefficients. With the Fourier domain approach attention can be focused on a particular frequency with high signal power, leading to more stable and easily interpretable maps (Gough and Ingham, 1983). An example of a Fourier transform event map is given in Figure 10 for the land part of the EMSLAB array (Gough et al., 1989). This figure illustrates both the value of event maps, and some of the problems associated with them. In this map of H_y amplitudes (i.e., the east-west component of the magnetic fields) there is a clear ridge of high amplitude extending north-south under the Cascade volcanic arc (filled triangles, Figure 10). This delineates a zone of enhanced conductivity,

a portion of which was already known as the Southwestern Washington Cascades Conductor (SWCC) from earlier work in this area (Law et al., 1980; Stanley, 1984). However, the complete map is very complicated, with many other features that could represent additional structures in the crust or mantle, complications in the source fields, or just noise. As noted by Gough (1989) interpretations based on single events can easily be misleading. Features need to appear repeatedly over many events, and remain stationary to be indicative of Earth structure.

One refinement of the event maps is to formally separate the magnetic fields into internal and external components. This can be accomplished with an integral transform of the total observed magnetic fields (e.g., Porath et al., 1970; Rokityanski, 1982). Implementation as a regularized inverse problem, where the unknowns are internal and external scalar magnetic potentials, is a natural extension (Richmond and Baumjohann, 1983). With this approach interpolation of the data onto a regular grid and field separation are accomplished in a single step. Some more recent discussion of internal/external separation are given by Viljanen et al. (2000), who use a novel set of spatially localized basis functions (spherical elementary current systems; Amm and Viljanen (1999)) to parameterize the internal and external magnetic fields. In principle, field separation should allow one to better identify anomalous features in the fields that are really internal to the Earth, and to define more quantitatively the spatial spectrum of inducing source fields. A major difficulty with any separation approach is that fields with spatial wavelengths exceeding the extent of the array cannot be separated uniquely. This difficulty lead Gough (1973) to conclude "... there is little advantage in the formal field separation as compared with an estimation of the normal field by smoothing the map or profile, and of the anomalous field as the difference between the original and smoothed maps or profiles". We note here that Gough's conclusions are based on experience with regional scale arrays mostly at mid-latitudes, and at periods from a few minutes to an hour or so. In these circumstances typical source wavelengths generally exceed array dimensions (Bannister and Gough, 1978), limiting the value of formal separation procedures. In other circumstances (higher latitudes, arrays covering larger areas, and over a broader frequency range) formal separation can be more useful (e.g., certainly at the global scale).

3.2. INTER-STATION TFS

Inter-station TFs provide a natural way to merge data from a number of events and to estimate the spatial pattern of laterally varying fields of internal origin. As for the MT impedance it is assumed that the external fields are essentially uniform (in some statistically averaged sense at least), so that any persistent lateral variations in amplitude and phase of horizontal magnetic fields are due to induced internal currents. For truly uniform sources the two horizontal magnetic components at any reference site ($\mathbf{h}_r$) exactly determine the magnetic fields at any other site ($\mathbf{h}_k$) (Schmucker, 1970; Egbert and Booker, 1989)

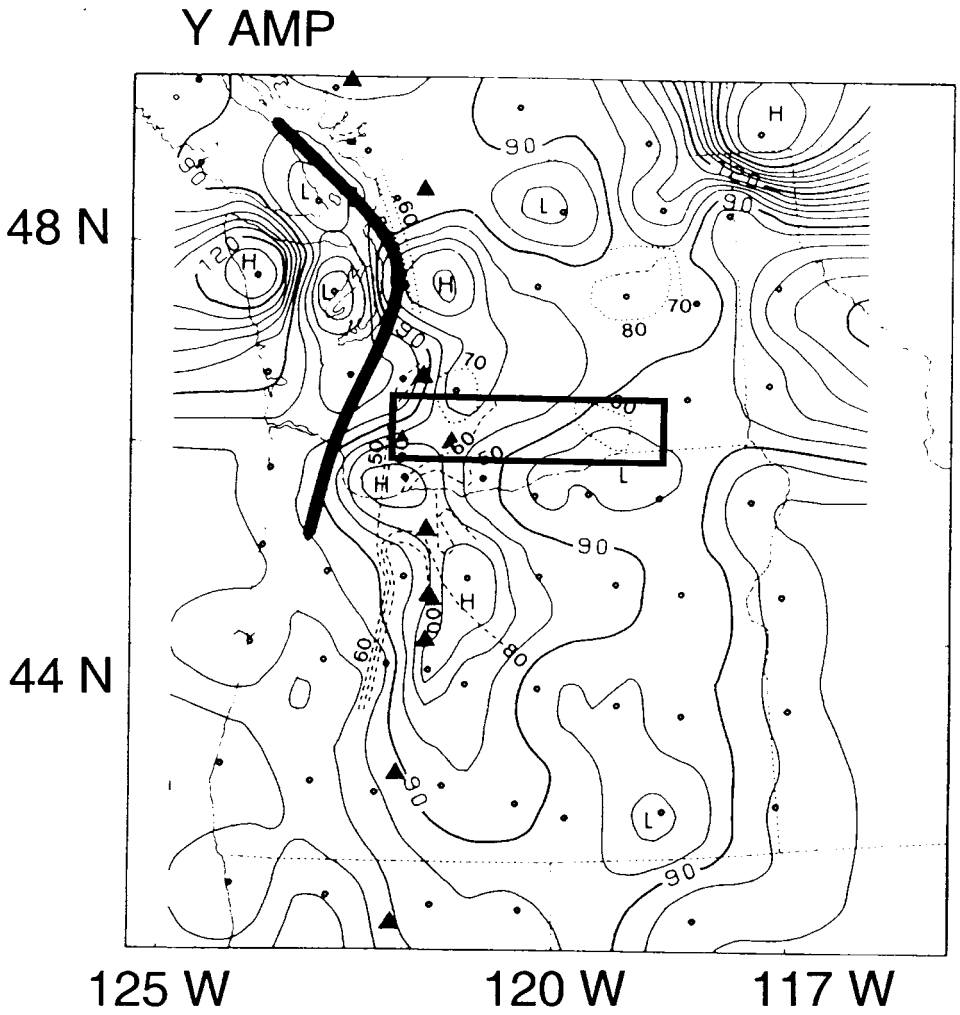

Figure 10. Event map from the EMSLAB array, from Gough et al. (1989). Here amplitude of the Fourier coefficients of the E–W magnetic field are plotted for a period of 18 min. The broken lines show heat flow contours (from Blackwell et al, 1982; 1985), the filled triangles are major Cascade volcanos, and the heavy solid line is the inferred 60 km depth contour of the subducting Juan de Fuca plate. Note the elevated amplitudes in an elongated zone over the cascades (the SWCC), and in the northeastern corner of the array. The rectangle gives the location of the four station MV array of Figure 12.

$$\mathbf{h}_k = \mathbf{T}_{kr}\mathbf{h}_r + \epsilon. \tag{8}$$

The 3×2 frequency dependent inter-station TF $\mathbf{T}_{kr}$ can be estimated exactly as for the MT impedance; robust, remote reference, and multivariate methods can be used. Each column of $\mathbf{T}_{kr}$ is a three component complex vector giving the complex amplitude of the magnetic fields that would be observed (on average) at site k when

the horizontal fields at the reference site r are of unit magnitude and linearly polarized (in the x and y directions, respectively for the two columns). In particular, for uniform sources over a laterally uniform Earth the upper 2×2 block of $\mathbf{T}_{kr}$ would be the 2×2 identity matrix $\mathbf{I}$, and the bottom row would be zero. If the reference site can be taken to be "normal" – i.e., in an area unaffected by lateral resistivity variations – deviations from this simple form give the "anomalous" fields, due to resistivity variations near site k (Schmucker, 1970). In practice, choice of a normal reference site is generally difficult, if not impossible.

The multivariate formalism of Egbert and Booker (1989) provides a useful perspective on inter-station TFs. Assuming that sources are uniform, the response space has dimension $M = 2$. The two vectors $\mathbf{u}_1, \mathbf{u}_2$ give the total magnetic (and electric) fields corresponding to two independent uniform external source polarizations (which are in general elliptical). Since we observe only total magnetic fields (internal plus external) the actual polarization of the external sources associated with each response vector is indeterminate without some additional information. Knowing that a particular reference site is normal (as defined above) would suffice, since at the normal site the polarization of the external and total fields would be identical. More realistically, the data only constrain the response space (i.e., the span of the columns of $\mathbf{U}$), and not specific response vectors $\mathbf{u}_x$, $\mathbf{u}_y$ associated with external sources linearly polarized N-S, E-W. Taking the horizontal magnetic components at the first site as a reference, and partitioning the matrix $\mathbf{U}$ into an upper 2×2 block $\mathbf{U_1}$ and lower $(K-2) \times 2$ block $\mathbf{U_2}$ (so $\mathbf{U}^T = (\mathbf{U_1}^T\ \mathbf{U_2}^T)$), we obtain a $(K-2) \times 2$ matrix $\mathbf{T}$ relating all other components in the array (electric as well as magnetic) to the two reference magnetic channels

$$\mathbf{T} = \mathbf{U_2}\mathbf{U_1}^{-1}. \tag{9}$$

With the multivariate formulation it is clear that normal fields can be defined in a more general way. For example, if we assume that all sites might be affected to some extent by internal anomalous magnetic fields, we can take the average magnetic fields as normal. This is accomplished by finding linear combinations of the response vectors $\mathbf{u}_1$ and $\mathbf{u}_2$ for which the average polarization is of the desired simple form – i.e., linearly polarized N-S and E-W. For 3-component data in a J station array, if we take

$$\mathbf{u}_1^0 = \left[J^{-1}\,0\,0 \mid \ldots \mid J^{-1}\,0\,0\right]^T \qquad \mathbf{u}_2^0 = \left[0\,J^{-1}\,0 \mid \ldots \mid 0\,J^{-1}\,0\right]^T \tag{10}$$

and set $\mathbf{U}_0 = \left[\mathbf{u}_1^0\ \mathbf{u}_2^0\right]$, we would estimate $\hat{\mathbf{u}}_x, \hat{\mathbf{u}}_y$ (i.e., the array response to unit magnitude linearly polarized normal fields) as

$$\left[\hat{\mathbf{u}}_x\ \hat{\mathbf{u}}_y\right] = \mathbf{U}(\mathbf{U}_0^T\mathbf{U})^{-1}. \tag{11}$$

Egbert and Booker (1989) provide further details.

In Figure 11 we give an example of the inter-station TFs obtained by applying the multivariate approach to a 4 site array of 3 component magnetometers. The array is in Southwestern Washington state, and straddles the SWCC, which coincides with the northern end of the conductive feature under the Cascades suggested by the high amplitudes in the event map of Figure 10. For this example we have taken the average fields to be normal, and estimated anomalous fields using (10)–(11). In this small array over a significant conductivity anomaly it is unlikely that any single site can be taken as normal. Assuming that average fields are normal is also questionable here, but this choice is at least independent of any specific site, and serves to emphasize that only relative variations in anomalous horizontal magnetic fields can be determined by array data. This indeterminacy obviously needs to be allowed for in any interpretation. Note that the vertical components given as numbers next to the sites in Figure 11 are not the usual single station vertical field TFs. Rather, these correspond to the vertical fields that would be seen when the *average* horizontal magnetic fields are linearly polarized N–S and E–W. If electric fields are included in the array, electric field components (relative to array averaged horizontal magnetics) would also be determined at each site (Egbert and Booker, 1989).

Interpretation of inter-station TFs in terms of lateral resistivity variations depends rather critically on the assumption that the external source fields are uniform over the array. As we shall show in Section 4, this assumption breaks down for large arrays (such as the EMSLAB array of Figure 1) which resolve persistent large scale features in geomagnetic variations. More surprisingly, this assumption can also break down in relatively small arrays at some periods. As a rather dramatic example, we return to the two station SAO/PKD array in California used for the eigenvalue plot of Figure 5 (Egbert et al.; 2000). In Figure 12 we plot amplitude and phase of the inter-station magnetic transfer function component T_{xx}, which gives H_x at the northern site (SAO) relative to H_x at PKD, 150 km to the south. As noted above, this array is generally contaminated by coherent noise from the BART DC train system. However, the TFs plotted in Figure 12 were calculated using data from a one week period when the train system was shut down due to a labor strike, and data from this time window appear to be relatively uncontaminated by coherent noise (Egbert et al. 2000). Very dramatic narrow band variations in both amplitude and phase are seen in the inter-station TF. Egbert et al. (2000) showed that these features in the TFs almost certainly result from local field line resonance associated with Pc3 geomagnetic pulsations (e.g., Chen and Hasegawa, 1974). Because the resonant period of Alfven waves propagating along field lines depends strongly on geomagnetic latitude, amplitudes (and phases) of the magnetic field variations also depend strongly on geomagnetic latitude near the resonant period for a particular latitude (Waters et al., 1991). The result is systematic biases in inter-station TFs near the resonant period for stations separated by 100 km or so. In addition to the fundamental resonant mode at 15s period, there is evidence for bias due to

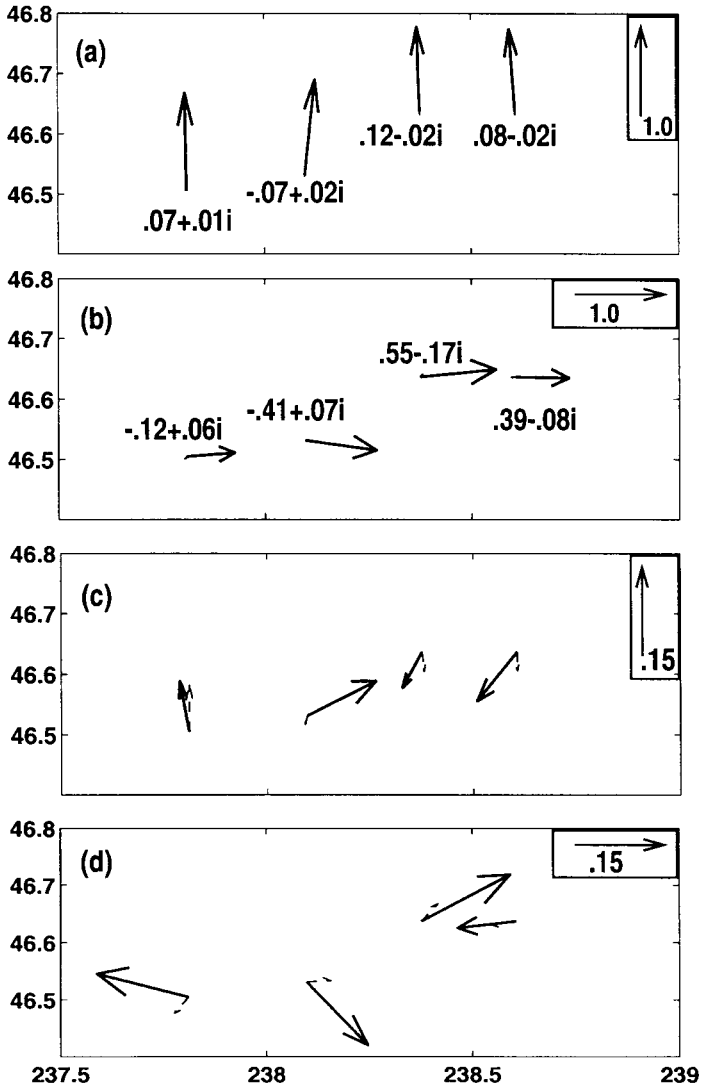

Figure 11. Inter-station TFs, or hypothetical events computed for a four station magnetometer array using the multivariate approach of Egbert and Booker (1989), for a period of 300 s. The array is located in the rectangle marked in Figure 10, and crosses the SWCC in the Cascade mountains of Southwestern Washington. Here we assume that the average horizontal magnetic fields are "normal". Solid arrows (with bases at the station locations) are real parts of the horizontal magnetic fields, dashed arrows are imaginary. Vertical components are written under the site location. In (a) the average fields are polarized N–S, and in (b) E–W. Variations of horizontal fields between sites are fairly subtle and hard to distinguish. The anomalous fields (with the assumed normal averages subtracted) are plotted in (c) and (d). There is a significant amplification of the E–W component in the center of the array, consistent with the sign reversal in the vertical components. Note that the relative enhancement of the E–W component in the center of the profile is evident in both source polarizations, suggestive of channeling of currents through the N–S trending SWCC (Egbert and Booker, 1993).

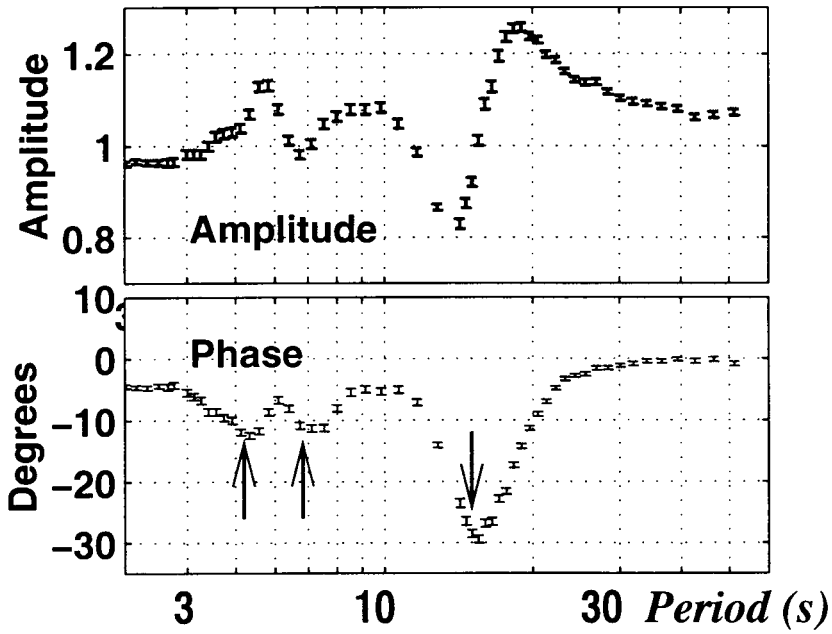

Figure 12. Relative amplitude and phase of H_X for the SAO/PKD array, computed for very closely spaced frequencies for days 252-257, 1997, a time when the DC electric railway in the San Francisco Bay Area was shut down due to a labor strike (after Egbert et al., 2000). The two sites are separated by a distance of 150 km, centered at a geomagnetic latitude of about 40 degrees. Rapid variations of inter-station TFs with frequency can be traced to the short spatial scales associated with Pc3 geomagnetic pulsations. The pronounced phase low at 15 s defines the average resonant period for field line oscillations at the latitude of the array midpoint (Waters et al., 1991). The other two phase lows occur at periods appropriate for the first two harmonics of the fundamental mode.

harmonics of the field line resonance at approximately 1/2 and 1/3 the fundamental period (Figure 12).

It is not clear how common these sorts of narrow-band source bias problems might be in general. For Figure 12 the interstation TF was estimated from a fairly long time series (about 6 days) with very high frequency resolution (over 40 bands in one decade), so that the systematic narrow-band biases are clear. With the frequency resolution of 5–8 bands per decade more commonly used in induction studies, the local resonance peaks would not be clearly resolved, but would rather create the appearance of noisy TF estimates over the band from 3–30 s. Further careful narrow-band array studies of source characteristics are clearly warranted.

In general local MT impedances are considerably less sensitive to source inhomogeneity than inter-station TFs. For MT impedances persistent gradients at scales much greater than a skin depth should have little or no biasing effect (Dmitriev and Berdichevsky, 1979). For example, MT impedances estimated for the two sites in the array just considered in Figure 12 showed little evidence of any significant source effects (Eisel and Egbert, 2001). Similarly, in the BEAR ar-

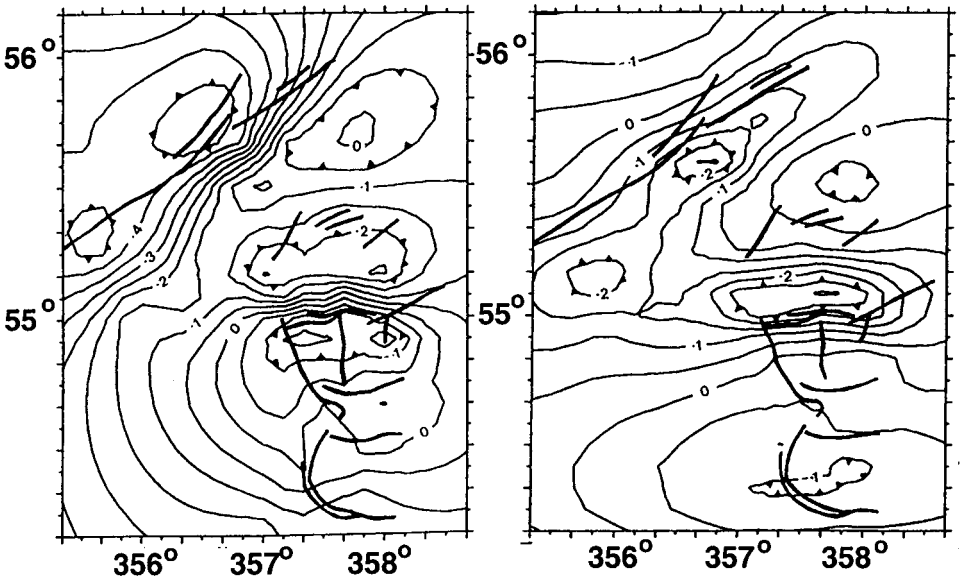

Figure 13. (a) Vertical field hypothetical event for the Northumberland Trough–Southern Uplands area in Northern England, constructed from single site TFs with correction for anomalous horizontal fields derived using the iterative scheme described by Banks et al. (1993). The real part of the vertical field response to geographic N–S source fields is contoured. (b) Real part of anomalous H_x hypothetical event map constructed from the single site vertical field TFs. (After Banks et al., 1993.)

ray, MT impedances were considerably less sensitive to source characteristics than inter-station TFs (Varentsov et al., 2001). However, inter-station TFs for reasonably nearby sites are likely to be at least as robust to assumptions of source uniformity as local vertical field TFs. In contrast to MT impedances, gradients in the source fields would be expected to have a similar first order effect on both sorts of TFs.

3.3. HYPOTHETICAL EVENT ANALYSIS

Hypothetical event analysis (HEA) was introduced by Bailey et al. (1974) as a simple way to display magnetovariational data from an array of non-simultaneous sites. In the classical approach, the two components of local site vertical field TFs (T_{zx} T_{zy}) are contoured. These vertical field maps are then interpreted as the anomalous vertical fields that would be seen for a pair of uniform source "hypothetical events" with orthogonal linear polarizations (in the x and y directions). However, since the vertical field TFs are usually computed relative to local magnetic fields, and not to a common reference, these maps only approximate the vertical fields that would be observed for true linearly polarized uniform sources. A refined HEA is possible with an array, since a common (and approximately normal) reference site can be used for calculation of inter-station vertical field TFs (Beamish and Banks, 1983; Arora et al., 1998). This display of single-site (or inter-station) vertical

field TFs has proven so effective that much recent interpretation of large two-dimensional simultaneous arrays has been based primarily on HEA (e.g., Gough et al., 1989; Chamalaun et al., 1999; Wang and Lilley, 1999; Arora et al., 1999).

Banks (1986) and Banks et al. (1993) proposed an iterative scheme to correct single station vertical field TFs for the effect of anomalous horizontal fields. Starting from interpolated vertical field maps from the classical single-site HEA, horizontal components of anomalous magnetic fields are computed and used to adjust vertical field TFs to a common reference (Figure 13). The procedure is repeated using the modified HEA, and iterated to convergence. One advantage of this approach is that it yields estimates of horizontal anomalous magnetic fields, even when a complete simultaneous array is unavailable (Figure 13).

For arrays it is possible to extend the HEA to directly estimate all components of the vector magnetic (and electric) fields associated with linearly polarized sources. Indeed, the uniform source response vectors $\mathbf{u}_x$ and $\mathbf{u}_y$, defined above in our discussion of the multivariate approach, are hypothetical events for all components in the array (electric as well as magnetic). Standard (or remote reference) processing could also be used to estimate TFs for all components relative to a fixed reference and the results combined to form estimates of $\mathbf{u}_x$ and $\mathbf{u}_y$ (e.g., Beamish and Banks, 1983; Banks, 1986; Banks et al., 1993). If two arrays run at different times share a common station, this site can be used as a reference to define a common hypothetical event for both arrays. The same idea can obviously be used to merge any number of overlapping arrays (Beamish and Banks, 1983). Egbert (1991) developed an optimal array combining scheme, which allows for multiple overlaps between arrays. Complete three component hypothetical events (or response vectors) built up by applying this scheme to a series of overlapping small arrays from Southwestern Washington (Egbert and Booker, 1993) are given as an example in Figure 14. Note that sites used as a common reference need not be used to define the normal reference fields. Once all stations are combined into a pair of uniform source response vectors $\mathbf{u}_1$ and $\mathbf{u}_2$, we are free to define the normal reference fields in any way we choose; e.g., defining the average fields to be normal, as in Figure 14. A recent example of a similar complete HEA based on non-simultaneous arrays from the Chilean Andes is given by Soyer and Brasse (2001).

As Figure 14 illustrates, the full set of inter-station TFs allows a complete three-component HEA, combining all available data into a statistically averaged estimate of the response of the array to sources of the largest scales. Maps obtained by HEA delineate conductive and resistive features much more clearly than simple actual event maps such as Figure 10. As discussed in Ritter and Banks (1998) HEA can also be used to separate local galvanic distortion of magnetic fields from regional induction effects. This allows estimation of a regional strike, and regional MT impedance phase from MV data (Ritter and Banks, 1998). By understanding the relative contribution of regional inductive and local galvanic contributions to observed anomalies more effective modeling and interpretation strategies can be

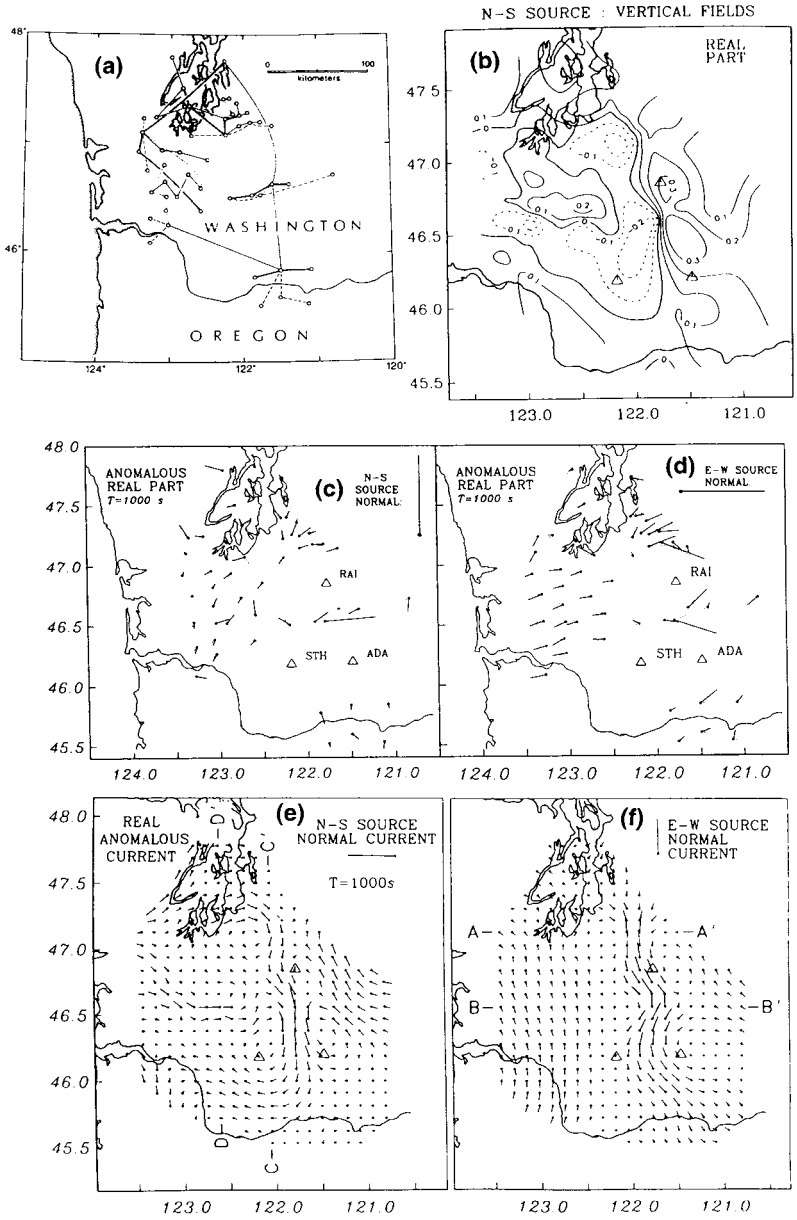

Figure 14. Examples of uniform source horizontal field hypothetical events for the Southwestern Washington area, after Egbert and Booker (1993). (a) Small (3–5 station) overlapping arrays used for the analysis, showing array connections. (b) Vertical field hypothetical event for the merged array. Note that all field components are given relative to the same normal fields at all sites (not relative to local horizontal components). (c–d) Anomalous horizontal field hypothetical events, with normal fields assumed equal to the average. (e–f) Interpolated equivalent horizontal sheet current that is consistent with both horizontal and vertical anomalous fields. Note the intense flow of current in the SWCC beneath the Cascade volcanos (for both source polarizations). There is a second smaller E–W trending anomaly in the western part of the array visible in (e).

devised (Arora et al., 1999). This sort of analysis is most effective if the HEA is based on inter-station, instead of single site TFs (Ritter and Banks, 1998). Use of the full three component HEA is not common, but should offer further advantages.

For an array of EM instruments the full response of the Earth to excitation by spatially uniform sources is contained in the complete hypothetical events or response vectors $\mathbf{u}_x$ and $\mathbf{u}_y$. In addition to the usual local TFs (impedances and vertical field TFs), the full response also contains information about anomalous horizontal field variations. The value of this information should be comparable to that in single site vertical field TFs. Since horizontal anomalous fields are indicators of current flow under a site, while vertical anomalous fields are indicators of currents off to the side (e.g., Banks, 1986), use of both seems likely to result in improved resolution. So far inversion methods for MT data have generally been developed to fit only the local TFs. The need is clear for more general inversion codes that incorporate all available information into the final interpretation. In principal this extension should be straightforward.

Maps of anomalous horizontal fields also may make some novel approximate imaging schemes feasible. As an example, Zhdanov et al. (1996) describe an EM migration scheme which requires both magnetic and electric fields on the surface. The complete hypothetical events that can be derived from full component TF analysis of array data provide just what is needed as input data for this sort of scheme. As another example, Egbert and Booker (1993) developed and applied a simple linear scheme to invert long period anomalous magnetic fields for integrated conductance of the crust.

4. Beyond Plane Wave Sources

4.1. Horizontal spatial gradient methods

When the external source magnetic fields have non-zero gradients, but still are of large scale compared to skin depths, the vertical magnetic fields over a one-dimensional layered Earth satisfy

$$H_z = C(\omega, 0)\left[\partial_x H_x + \partial_y H_y\right] = \frac{-iZ(\omega)}{\omega}\left[\partial_x H_x + \partial_y H_y\right], \tag{12}$$

where $Z(\omega)$ is the usual 1-d MT (plane wave) impedance. The complex inductive response function $C(\omega, k)$ has units of length, and in general depends on the wavenumber k of the inducing fields. In the limit $k \rightarrow 0$, where source wavelengths are large compared to penetration depths, the explicit wavenumber dependence may be ignored and $C(\omega, 0)$ is proportional to the usual uniform source scalar impedance appropriate to a one-dimensional Earth. Equation (12) provides the basis for the horizontal spatial gradient (HSG) method (Schmucker, 1970; Kuckes, 1973a,b; Lilley et al., 1976; Jones, 1980), which allows computation of an equivalent scalar MT impedance without measuring electric fields.

For specialized sources where the spatial structure is assumed known, the HSG method can be applied to data from single sites or very small arrays. In these cases gradients of the horizontal magnetic fields are not explicitly calculated, though the basic physical principal remains as expressed in (12). The key assumption required for single site HSG is that the source fields contain a single known spatial mode, so that local measurements of the horizontal magnetic fields at one location suffice to completely define the source fields. The most familiar example is the so-called Z/H method used to estimate impedances at periods longer than about 5 days. In this case the assumed single external source is the magnetospheric ring current in the (geomagnetic) equatorial plane, associated with the recovery phase of Dst. This source produces fields on Earth's surface that are well described by a P_1^0 spherical harmonic, at least at mid-latitudes (Banks, 1969; Schultz and Larsen, 1987; Banks and Ainsworth, 1992). As another example, Bahr and Filloux (1989) applied this general approach to Sq variations observed at EMSLAB sea-floor sites to estimate equivalent 1-d impedances at $m = 1, 2, 3$, and 4 cpd. Here the sources are assumed to be well modeled by the P_{m+1}^m spherical harmonic (with a small correction to allow also for a P_{m+3}^m component), and ratios of H_z to H_y are used to estimate an equivalent 1-d impedance.

Use of the HSG approach in more general circumstances requires a large simultaneous array, so that actual gradients of the horizontal fields can be estimated. Jones (1980) discusses estimation of $C(\omega, 0)$ using spatial gradients in the IMS magnetometer array (Küppers et al., 1979). Quadratic polynomials were fit in the frequency domain to horizontal and vertical magnetic fields at 10 sites in Northern Scandinavia. Estimates of $\partial_x H_x + \partial_y H_y$ and H_z at the origin of the array were obtained from the polynomial coefficients for each of a series of events and frequencies, and transfer function methods were applied to the series of coefficients to estimate the inductive response function $C(\omega, 0)$ in (12).

Olsen (1998) estimated $C(\omega, 0)$ for periods from 3–720 hours at geomagnetic observatories in Europe. Damped LS was used to fit magnetic fields from 90 globally distributed observatories to a truncated spherical harmonic expansion. Estimates of gradients were then obtained from the fitted fields, and used with the local H_z to estimate the inductive response functions at a number of locations. In this study approximate allowance was made for the wave number dependence of $C(\omega, k)$; see Olsen (1992, 1998) for details.

The theory behind the classical HSG method explicitly assumes that resistivity varies only with depth, so that the MT impedance is a scalar. Furthermore, if resistivity variations in the Earth are not exactly 1-d, anomalous internal magnetic fields can contaminate both the vertical fields and estimates of the gradients in the external fields (e.g., Beamish and Johnson, 1982; Bahr and Filloux, 1989). Thus even for long period studies where deeper mantle resistivity variations might be assumed to be relatively 1-d, distortion of currents by crustal heterogeneity (Chave and Smith, 1994; Ritter and Banks, 1998) can still contaminate HSG estimates, making the method difficult to apply in most environments. An extension of the

HSG approach beyond the classical 1-d case was outlined by Kuckes et al. (1985), but the suggested approach has apparently never been applied to actual data. We illustrate these ideas in the next section in the context of a specific example, the EMSLAB magnetometer array of Figure 1 (Gough et al., 1989).

4.2. SPATIAL GRADIENTS IN THE EMSLAB SRRAY

The EMSLAB array data were collected with analogue instruments, and in many respects are not of the quality that can be achieved with modern digital instruments. However, this array still provides a good illustration of several important points, and suggests areas for further research on gradient methods. Our analysis here is based on application of the multiple station approach of Egbert and Booker (1989), Egbert (1989a) and Egbert (1997), to the 60 hours of digitized array data described in Gough et al. (1989). Data for 55 three component magnetometer sites are used in our analysis, for a total of 165 data channels.

In Sections 2 and 3 we considered use of the multivariate approach for estimation of local and inter-station TFs. Here we apply multivariate methods to a more exploratory analysis of the spatial structure of sources in the EMSLAB array. In this application the method is a frequency domain analogue of empirical orthogonal functions (EOFs), in which the primary goal is to estimate the dominant coherent spatial modes in the array. Eigenvalues of the spectral density matrix (SDM) computed for a period of 1000 s are plotted in Figure 15. For this plot we have normalized the eigenvalues by total signal power. A large fraction of the total variance is explained by a small number of spatial modes, with 98.9% accounted for by the first 6 eigenvectors of the SDM (Figure 16). To a good approximation the first two modes $\mathbf{w}_1$, $\mathbf{w}_2$ are uniform across the array. Modes 3–5 are dominated by gradients in the horizontal magnetic fields, while mode 6 has a somewhat noisier appearance. In the context of our multivariate model (5) the dimension of the source space is approximately $M = 5$ or 6 (assuming that there are no very large scale coherent sources of noise, as seems reasonable here).

Focusing initially on the first two modes, and assuming that the average horizontal fields are normal, we can obtain estimates $\tilde{\mathbf{u}}_x$, $\tilde{\mathbf{u}}_y$ of the total fields resulting from spatially uniform sources polarized linearly N-S and E-W. These are computed (in geomagnetic coordinates) as linear combinations of $\mathbf{w}_1$ and $\mathbf{w}_2$, using Equations (10)–(11) (Figure 17(a–b)). The anomalous fields (i.e., differences from the average) show clear evidence for consistent source gradients in the estimated geomagnetic E–W source response $\tilde{\mathbf{u}}_y$ (Figure 17c). This shows that the two dominant modes of this large array are in fact a mixture of uniform and large scale gradient sources. HEA for plane wave sources thus cannot be based solely on the first two modes of the SDM. Interestingly, the geomagnetic N–S array response estimate $\tilde{\mathbf{u}}_x$ does not show nearly as much contamination by persistent source gradients.

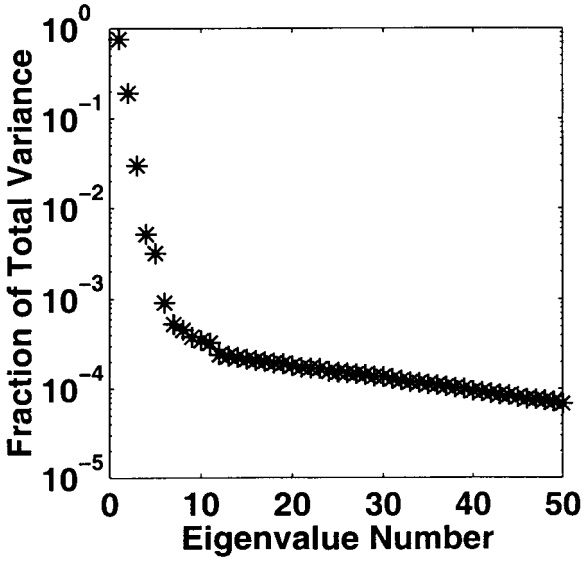

Figure 15. Eigenvalues of the normalized SDM computed for the EMSLAB land magnetometer array at a period of T = 1000 s. Sixty hours of digitized data were used for the analysis. There are 5–6 modes above a relatively constant background level. Here the eigenvalues have been normalized by the total signal power (i.e., the sum of all eigenvalues) to give the fraction of total variance associated with each mode. The first few modes account for almost all of the variance in the array.

To better understand the source gradients in the EMSLAB array we turn to the general theory outlined by Kuckes et al. (1985), and Egbert (1989a). The assumption of uniform sources is at best an approximation, appropriate when both the spatial extent of the array and skin depth are a small fraction of the source wavelength. The next level of approximation to the actual spatial structure of sources would allow for gradients in the horizontal magnetic fields. With two horizontal components this suggests four source components: $\partial_x H_x$, $\partial_y H_x$, $\partial_x H_y$ and $\partial_y H_y$. However, from Ampere's Law $\nabla \times \mathbf{H} = \mathbf{J}$, and since there is no vertical current flow through the surface of the Earth, we must have $\partial_x H_y - \partial_y H_x = 0$, i.e., the horizontal magnetic fields must be curl free. Thus there are only three independent gradient components. Kuckes et al. (1985) point out that the most natural set of basis functions to define the allowable three independent horizontal magnetic gradients are

$$\mathbf{h}_3(x, y) = \begin{bmatrix} x \\ y \end{bmatrix} \qquad \mathbf{h}_4(x, y) = \begin{bmatrix} x \\ -y \end{bmatrix} \qquad \mathbf{h}_5(x, y) = \begin{bmatrix} y \\ x \end{bmatrix}, \tag{13}$$

where the two components of each vector field define the H_x and H_y components of the magnetic fields, and (x, y) are coordinates with respect to an origin at the center of the array. The coefficients of these basis functions in a Taylor series expansion of the curl-free horizontal magnetic fields around the coordinate system origin are given in terms of gradients of the magnetic fields as

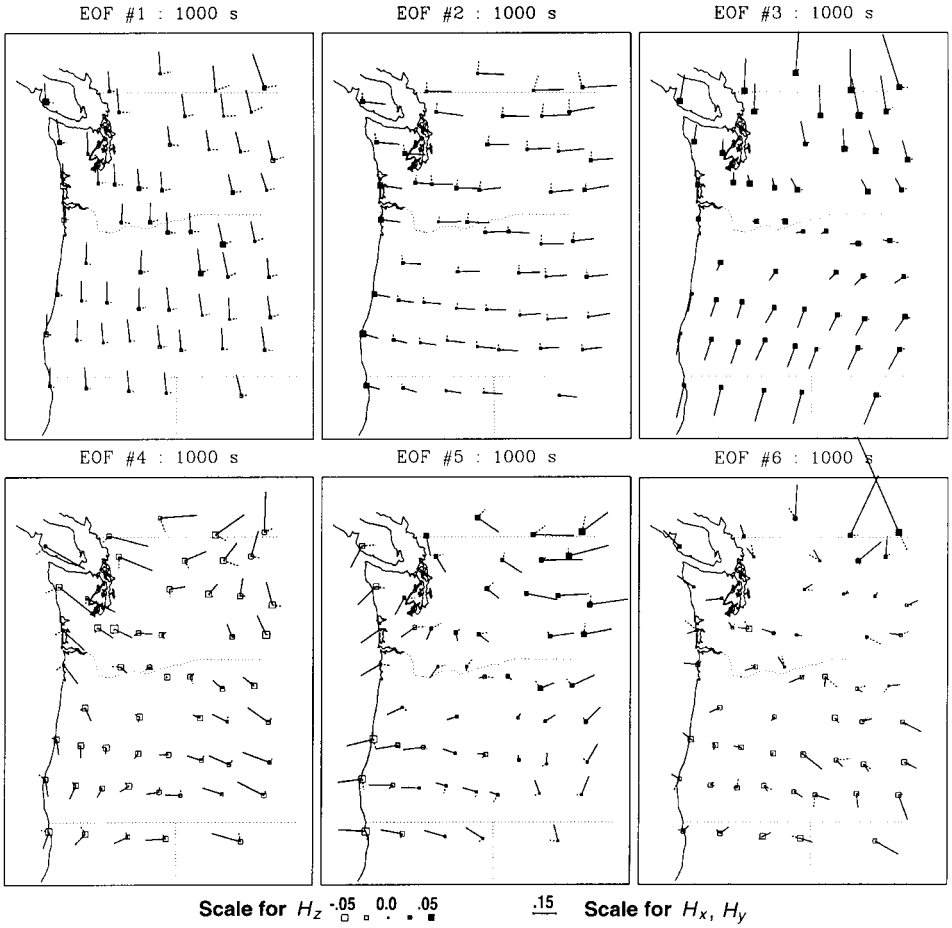

Figure 16. Eigenvectors (EOFs) associated with the largest eigenvalues of the EMSLAB array SDM. The first two modes are roughly uniform across the array. Modes 3–5 are dominated by large-scale gradients in the magnetic fields. Mode 6 has a significantly noisier appearance, but also shows evidence of coherent large-scale gradients.

$$\partial_x H_x + \partial_y H_y \qquad \partial_x H_x - \partial_y H_y \qquad \partial_x H_y + \partial_y H_x. \tag{14}$$

The first of the gradient components is invariant under rotations. The second two components are related by rotation; $\mathbf{u}_5$ is obtained by a clockwise rotation of 45 degrees of $\mathbf{u}_4$ (see Figure 18). Changing coordinate systems thus leaves the coefficient of $\mathbf{u}_3$ fixed, and mixes the coefficients of $\mathbf{u}_4$ and $\mathbf{u}_5$ (Kuckes et al., 1985).

The uniform source excitation assumed for most traditional TF methods can be similarly expressed as

$$\mathbf{h}_1(x, y) = \begin{bmatrix} 1 \\ 0 \end{bmatrix} \qquad \mathbf{h}_2(x, y) = \begin{bmatrix} 0 \\ 1 \end{bmatrix}. \tag{15}$$

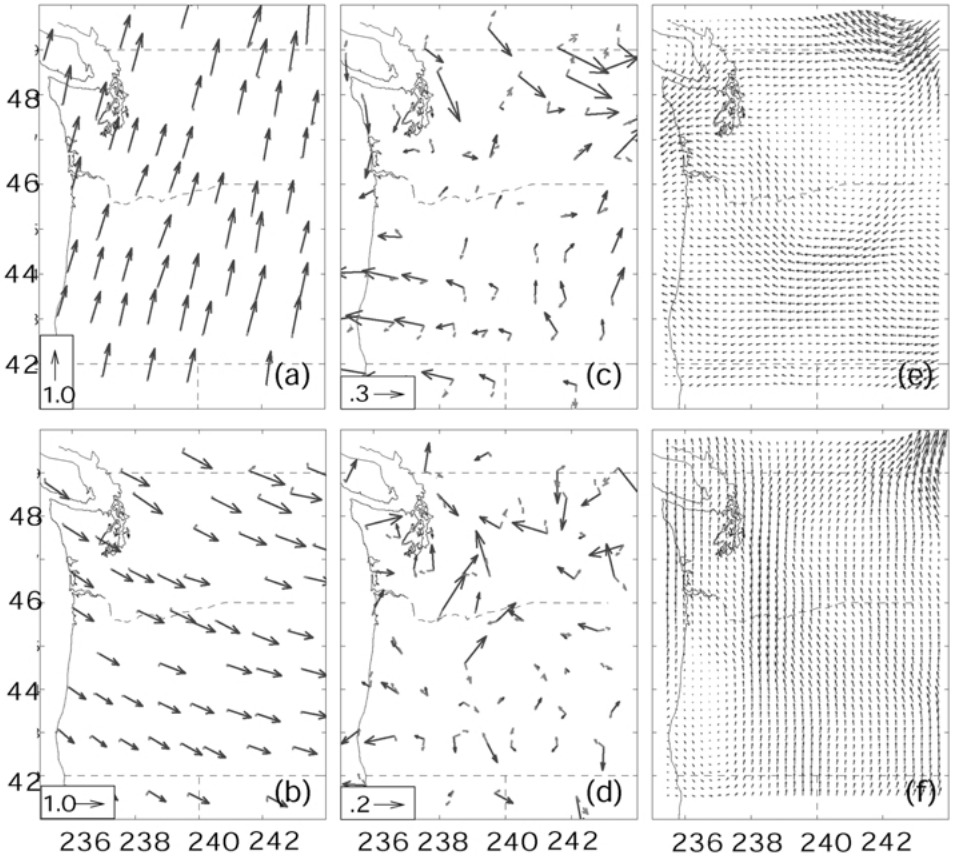

Figure 17. (a–b) Estimates of the uniform source response (hypothetical events) obtained by taking linear combinations of the first two EOF modes from Figure 16, with the constraints that the average horizontal magnetic fields are linearly polarized N–S and E–W (in geomagnetic coordinates). Note the significant N–S gradient for the E–W polarization of (b). These large scale gradients, which are more clearly evident in (c) where anomalous fields are plotted, almost certainly reflect external source structure. (d) Anomalous horizontal fields for the E–W polarization computed as a linear combination of the first 6 modes, following the scheme discussed in the text do not exhibit the same large-scale gradients. (e–f) Smoothed equivalent sheet currents derived from fitting the estimated uniform source responses. In (e) normal magnetic fields are N–S (geographic now) and current flows from the E. In (f) normal magnetic fields are E–W, with current flowing from the south. Note the enhancement of electric current flow under the Cascades, and in the northeast corner of the array, the relatively resistive zones (smaller or reversed current flow) in the Columbia Basin and Oregon Coast range.

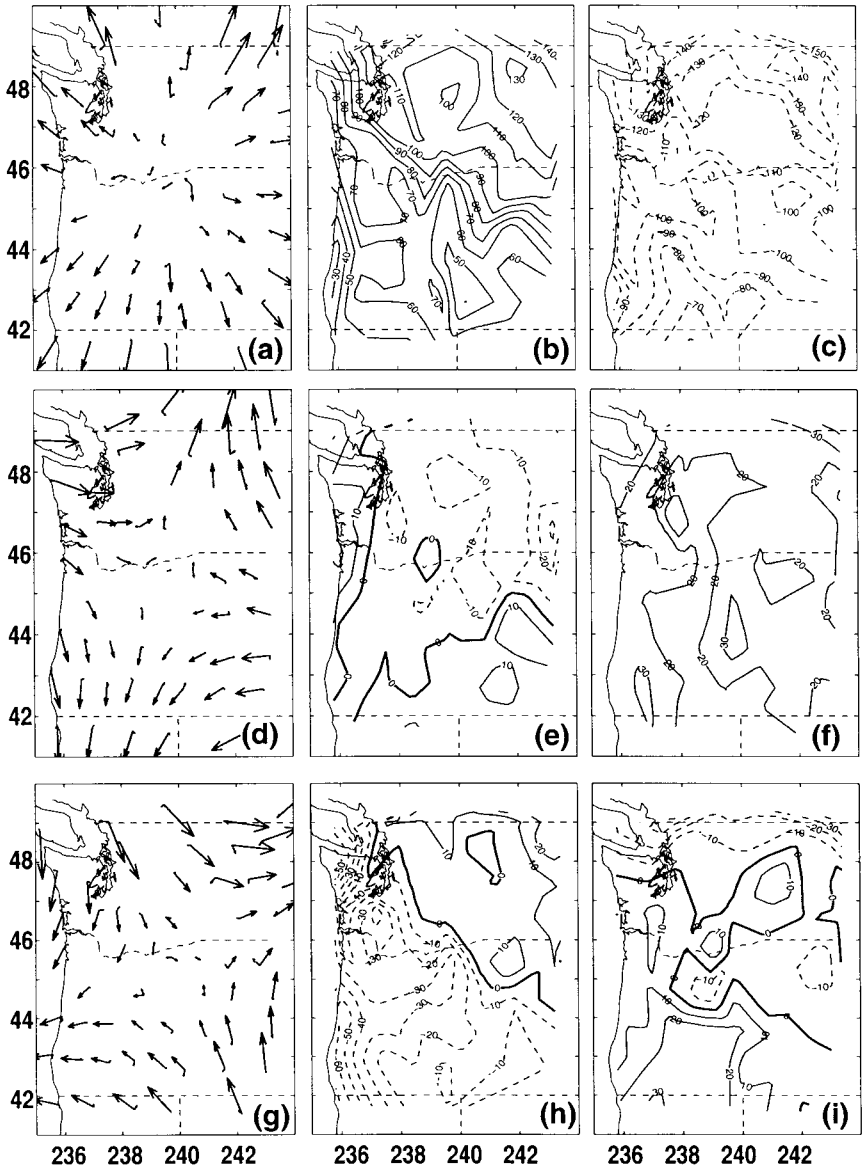

Figure 18. Canonical gradient response vectors obtained using the separation procedure discussed in the text. The first column gives horizontal magnetics, the second and third the real and imaginary parts of the vertical component. The first row (a-c) is the gradient response $\mathbf{h}_3$ normally used for the HSG approach. This gradient component is invariant under rotations of the horizontal coordinate system. The second and third rows correspond to a pair of gradient source terms ($\mathbf{h}_4, \mathbf{h}_5$) that rotate together (e.g., rotating (d) 45 degrees clockwise, yields (g)). Vertical fields are expressed in km, scaled into the complex inductive length scale; the scale on the horizontal field vectors is arbitrary here. For a 1-d Earth the vertical fields associated with $\mathbf{h}_4, \mathbf{h}_5$ should vanish. Although generally smaller than those associated with the first gradient source, vertical fields associated with $\mathbf{h}_4, \mathbf{h}_5$ do not vanish, as the would for a 1-d Earth.

The three curl-free uniform gradients of (13) thus provide three additional source excitations. The first of these, $\mathbf{h}_3$ is in fact the source used by the classical HSG method, in which the scalar response function $C(\omega, 0)$ is determined from the ratio of H_z to the complex coefficient $\partial_x H_x + \partial_y H_y$. Kuckes et al. (1985) proposed interpreting also the response of the Earth due to the additional curl-free gradient sources defined by $\mathbf{h}_4$ and $\mathbf{h}_5$. It is readily verified that over a layered 1-d resistivity structure there are no vertical fields excited by these sources (Kuckes et al., 1985). With lateral variations in resistivity this will no longer be true, and interpretation of the response of the Earth to these additional source functions may be expected to provide additional useful information about lateral resistivity variations.

The exact correspondence between the full 2×2 MT impedance tensor (appropriate to the general case of three-dimensional resistivity variations) and these three gradient response elements is unclear. A simple counting argument (4 complex parameters in the impedance tensor, vs. 3 gradient terms) shows that the correspondence cannot generally be exact. However, it should still be possible to invert and interpret estimates of these response parameters.

With this general background on gradient sources we return to the example of the EMSLAB array. The estimated uniform source response vectors $\tilde{\mathbf{u}}_x, \tilde{\mathbf{u}}_y$ plotted in Figure 17 were calculated from the two dominant eigenvectors of the SDM. Although uniform sources clearly dominate the first two eigenvectors (see Figure 16), the actual sources associated with these hypothetical events clearly also contain gradient components. Similarly, although modes 3–5 are clearly dominated by gradients, these must contain uniform source components as well. Since gradients due to the sampled internal anomalous fields may be confused with actual source gradients, an exact separation of the gradient and uniform source responses will be impossible. We use a simple heuristic scheme which allows at least an approximate separation, into hypothetical events associated with all 5 of the uniform and gradient source excitations.

Define $\mathbf{u}_m^0, m = 1, 5$ to be unit vectors of dimension K (= total number of components) with horizontal magnetic field components proportional to the idealized source functions $\mathbf{h}_m$ (defined in (13) and (15)), sampled at the array data sites. For the $K = 3J = 165$ component EMSLAB array $\mathbf{u}_1^0$ is proportional to $(1\,0\,0 \mid 1\,0\,0 \mid \ldots \mid 1\,0\,0)^T$, while $\mathbf{u}_3^0$ is proportional to $(x_1\, y_1\, 0 \mid x_2\, y_2\, 0 \mid \ldots \mid x_J\, y_J\, 0)^T$, where (x_j, y_j) are site locations (in km) with respect to the center of the array. Note that the vectors $\mathbf{u}_m^0$ are the uniform source and gradient response vectors corresponding to a laterally uniform Earth. We estimate the actual response vectors $\mathbf{u}_m, m = 1, 5$ as linear combinations of the $N = 6$ dominant eigenvectors of the SDM $\mathbf{w}_n$

$$\hat{\mathbf{u}}_m = \sum_{m=1}^{N} c_{nm} \mathbf{w}_n \tag{16}$$

by minimizing the estimated total error variance $\mathbf{Var}(||\hat{\mathbf{u}}_m||) = \sum |c_{nm}|^2 \sigma_n^2$ subject to the constraint that the horizontal magnetic components of the estimated response vectors are near what would be expected for a 1-d Earth:

$$\sum_{m,m'=1}^{M} = |\hat{\mathbf{u}}_m^* \mathbf{u}_{m'}^0 - \delta_{mm'}|^2 \leq T^2, \tag{17}$$

where $\delta_{mm'}$ is the Kronecker delta, T^2 is a specified tolerance, and σ_n^2 is an estimate of the variance in the n^{th} EOF mode (computed following the theory described in Egbert (1991; Appendix B)). This *ad hoc* separation scheme cannot be justified rigorously, but it provides a stable approximate division of the response space into uniform and gradient source components. This can be viewed as a generalization of Equation (9), which was used to define normal fields for plane wave sources, to allow the definition of normal fields for a more general HEA.

The estimated response vectors $\hat{\mathbf{u}}_m$ provide estimates of hypothetical events for five sources. Each has H_z components which give the pattern of vertical fields associated with the idealized source type, as well as anomalous variations in the horizontal fields. Anomalous horizontal fields are plotted for the E-W uniform source term in Figure 17d. The anomalous horizontal fields in this plot are rather difficult to interpret, in part because of the rather wide site spacing, and in part because the anomalous fields by definition average to zero. Figure 17e–f give estimates of smooth equivalent sheet currents which are consistent with the anomalous magnetic fields for both x and y source polarizations (now in geographic coordinates). Computation of the sheet current from the anomalous fields was accomplished as described in Egbert and Booker (1993), and in Figure 14. Briefly, anomalous horizontal and vertical magnetic fields were inverted for an optimally smooth internal magnetic potential (Egbert, 1989b), and the smoothed magnetic field vectors were then converted to an equivalent sheet current by rotating 90 degrees counterclockwise. A small constant normal current was added to the anomalous sheet current to enhance clarity of the figure (Egbert and Booker, 1993). Several significant features can be seen in this figure, which should be compared to the single event map of Figure 10. Most obvious are the strong concentration of northward flowing currents in the Southwestern Washington Cascades Conductor (Law et al., 1980; Stanley, 1984), and the intense concentration of current at the top left corner of the array in the previously mapped southern Alberta–British Columbia conductor (Gough, 1986). Areas of generally reduced (or reversed) current flow are evident in the resistive western part of the array in the Oregon Coast range, and in the Columbia Basin resistive block (Gough et al., 1989) in eastern Washington. These uniform source hypothetical events are generally supportive of the regional interpretation of Gough et al. (1989).

The estimated array responses for the three gradient sources are plotted in Figure 18. The horizontal components of the magnetic fields match the idealized source functions of (13) almost exactly. Comparing $\hat{\mathbf{u}}_5$ (Figure 18c) with Figure 16,

we see that the gradient contamination in the estimate $\tilde{\mathbf{u}}_y$ is almost completely from $\mathbf{h}_5$. This implies that spatially uniform E–W polarized magnetic sources ($\mathbf{h}_2$) are positively correlated with gradient function $\mathbf{h}_5$. The linear superposition $\mathbf{h}_2 + \epsilon\mathbf{h}_5$ (with ϵ small) corresponds closely to the pattern of magnetic variation vectors seen in Figure 17b, with amplitudes of the E–W component decreasing toward the south. This pattern of magnetic fields corresponds to an equivalent sheet current which diverges as it flows from north to south (in local geomagnetic dipole coordinates). A possible explanation is that the E–W magnetic variations are at least in part associated with field aligned currents connecting the auroral ionosphere to the magnetospheric ring current. An equivalent sheet current projected to the surface of the Earth associated with these currents would indeed systematically diverge for equator-ward flowing currents.

Real and imaginary parts of the vertical components of the estimated gradient response vectors are contoured in Figure 18d–i. As discussed in Egbert (1989a), if the response vectors are scaled so that the horizontal components are in kilometers (consistent with the centered site locations x_j, y_j) the vertical components will correspond to the complex inductive length scale (also in kilometers). As would be expected for this complex area with significant lateral resistivity contrasts, there are significant vertical components associated with all three gradient sources. The strongest vertical field responses are indeed associated with the $\mathbf{h}_3$ mode used in the classical HSG method. However, very large vertical fields are also associated with an apparent coast effect for the $\mathbf{h}_5$ mode.

Although the use of the "canonical" gradient basis advocated by Kuckes et al. (1985) is very elegant, alternative representations may in some cases be more useful. For example, defining

$$\mathbf{h}_x = \frac{1}{2}[\mathbf{h}_3 + \mathbf{h}_4] \qquad \mathbf{h}_y = \frac{1}{2}[\mathbf{h}_3 - \mathbf{h}_4], \tag{18}$$

$\mathbf{h}_x, \mathbf{h}_y, \mathbf{h}_5$ also form a complete basis for curl free gradient fields. This basis may have advantages for two-dimensional resistivity variations. If coordinates are chosen so that x is along the geoelectric strike, then excitation by gradient source $\mathbf{h}_y$ is purely TE mode, while excitation by $\mathbf{h}_x$ is purely TM mode.

Vertical fields for these two alternative gradient modes for the EMSLAB array are plotted in Figure 19. Although it is impossible to define a clear geoelectric strike for the entire area, we take the strike direction x to be geographic north, roughly parallel to the west coast of North America. The "TM" mode gradients (Figure 19a-c) show essentially no coast effect, while the effect of the ocean is clearly visible in the TE mode (Figure 19d–f). Vertical components for both modes are smallest in the southeastern corner of the array, consistent with a relatively shallower zone of high mantle conductivity beneath the basin and range (Gough et al., 1989). However, there are many complicating features in these figures. There is a strong tendency to larger amplitudes of H_z in the north. Most likely this reflects complications in the source, rather than resistivity variations in the

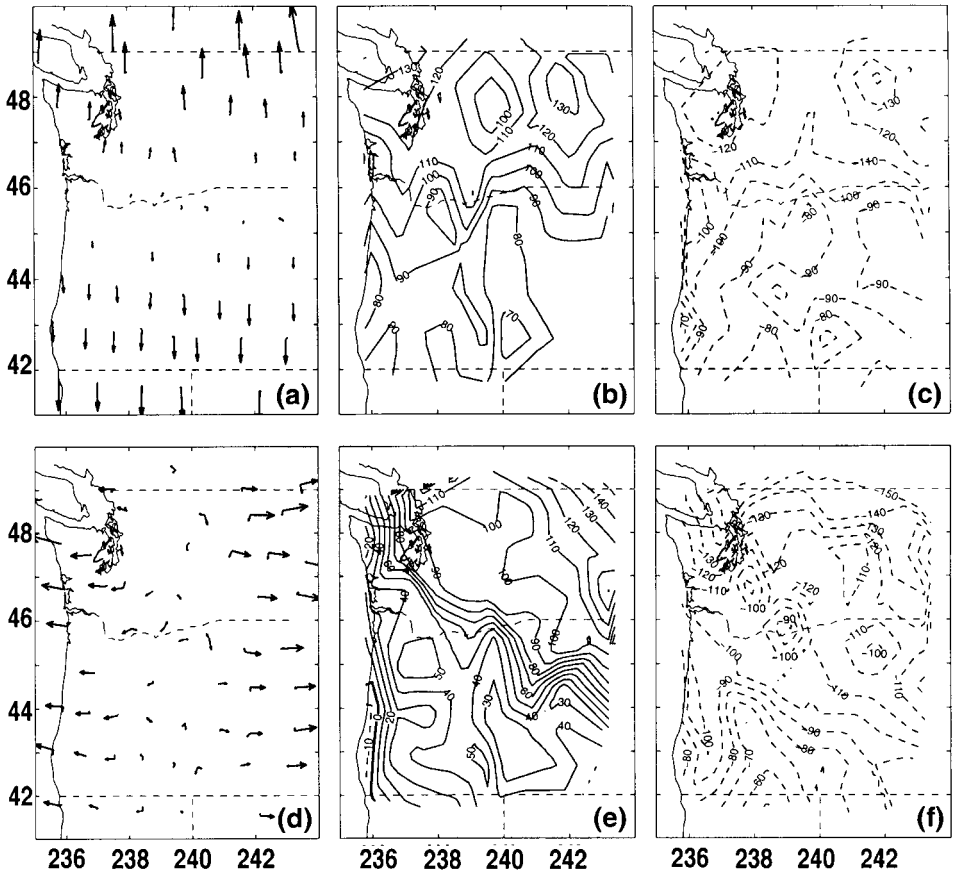

Figure 19. TM (a–c) and TE (d–f) gradient source terms, constructed as linear combinations of the canonical gradient terms of Figure 18. Here we have taken the overall strike of the region to be N–S, roughly coincident with the coast, the subducting plate, and the Cascade mountain range. The TM mode appears better behaved, with less contamination due to superficial conductivity anomalies (such as the ocean). Both modes are suggestive of a shallower zone of conductive upper mantle beneath the southwestern part of the array. The increase in amplitudes of vertical components at the top of the array is probably at least in part due to intensification of external sources further to the north.

Earth. Large scale vertical fields observed in any array can be due to external (or internal) current systems flowing well beyond the boundaries of the array. Also, in the classical HSG approach, vertical fields are all taken to be "normal". Just as for plane wave sources, lateral variations in resistivity will generate vertical (and anomalous horizontal) fields in a gradient response. For example the real part of the complex inductive length scale is negative near the coast in the TE mode. This would not be physically possible for $C(\omega)$ over a 1-d Earth (e.g., Jones, 1980), and arises due to concentration of N-S flowing currents in the ocean.

4.3. FUTURE DEVELOPMENTS OF HSG METHODS

The examples from the EMSLAB array presented here are far from definitive. They are based on analysis of a small amount (60 hours) of analogue data. Modern digital data sets (e.g., of the BEAR array, or the AWAGS array (Chamalaun and Barton, 1993)) would have many advantages for this sort of intensive statistical analysis. The response due to second order gradient sources will have significantly poorer signal-to-noise ratios than the uniform source response, and is likely to be much more sensitive to details of individual source events (which might be expected to be incompletely observed by an array of limited extent). The point of this example is to suggest that for large arrays methods can be developed which will allow more quantitative interpretation of a richer spectrum of external sources. The possibility of including electric field measurements (as with the BEAR array for example) also deserves consideration. Our hope in presenting these very preliminary examples from the EMSLAB array is to encourage others to further explore possibilities for quantitative interpretation of array data, going beyond the usual uniform source TFs, beyond the classical HSG method, and beyond the more qualitative array interpretation methods that were developed in the days of analogue instruments and limited EM modeling capabilities.

A major research question at this point is the degree to which quantitative interpretation of gradient sources can complement MT, and possibly reduce uncertainties about large scale static distortion. Depths of even large scale crustal and upper mantle features inferred from MT data can be seriously distorted by near-surface complications. Close site spacing allows near surface features to be imaged, and accounted for in interpretation of deeper structures. With widely spaced MT data these near surface complications will not be adequately sampled, and small-scale shallow structures may be aliased to large-scale deep structure. Mapping resistivity variations with depth using gradient approaches may provide some control over these static effects, which predominantly effect local electric fields. Of course there are complications (and dangers of aliasing!) in interpretation of magnetic variations as well. But joint interpretation of magnetic array response functions and MT might resolve large scale resistivity variations in the crust and upper mantle most reliably.

There are many issues that need to be addressed. Most importantly we need to develop modeling, and then inversion capabilities. At first blush this appears straightforward: the forcing for the forward modeling codes need only be modified to allow for more general external sources, while inversion requires some scheme to find a model which matches the data for these source geometries. However it is not obvious how boundary conditions should be implemented to account for pure gradient fields of the sort described here. For example, to what extent do details of the actual source distribution outside of the array effect observables, or modeling outputs? Data processing approaches also will need development. The analysis of the EMSLAB array presented here was essentially exploratory, intended

to demonstrate that most of the signal in the array could be well represented by a few modes corresponding to fairly simple source geometries. Methods for actual estimation of gradient response functions for 2-d and 3-d interpretation need much further development. Alternatives to the multivariate methods discussed here may be more useful for many purposes.

One approach would be to acknowledge from the outset that we do not exactly know source geometries. These need to be left to some extent as free parameters in the inversion stage. The multivariate analysis applied to the EMSLAB array can be viewed as a way to extract the dominant modes of variability in the array, without really making any explicit assumptions about source geometry. In effect, an EOF approach averages and condenses a number of actual events into a much smaller number of hypothetical events. The actual sources responsible for these hypothetical events are not exactly determined, but tend to be dominated by the largest (and hence most coherent) spatial scales. By averaging over many events small scale transient details in the external sources tend to average out, and signal-to-noise ratios are enhanced. In our specific example we found that sources can be at least approximately described by a simple and physically sensible set of basis functions, uniform and curl-free gradient fields. However, precise separation of these data modes (EOFs) into exactly known external sources was problematic. This uncertainty (and uncertainty about distant sources that might effect H_z within the array) should be allowed for in the inversion and interpretation process. Methods to do this are in need of much development.

5. Summary

The simultaneous nature of array data is useful for three general areas of application in induction studies: improvement of local TF estimates; computation of inter-station uniform source TFs; and allowing for more complex sources. For the first of these applications the widely used RR method for MT impedance estimation is fundamental, and this requires only two sites. Multiple site arrays allow some extensions of the basic RR estimate, but in many, if not most, cases these are second order refinements. Multiple sites allow improved definition of the reference fields, but in general cannot do anything about noise in the local **h** and **e** fields which more often limit estimation accuracy. Arrays can provide some useful diagnostics about coherent noise or other source complications, allowing the best data to be selected for processing. However, if the array is large enough to sufficiently resolve the source complexity, there is generally a remote site distant enough to provide adequate cancellation of the biasing noise. Exceptions to this general statement can certainly be found.

Inter-station uniform source TFs provide additional information about resistivity variations in the Earth. Horizontal anomalous fields have not been widely used in quantitative interpretations of MT, and in general MT inversion programs do

not allow for fitting these sort of parameters. There is no reason why estimates of horizontal anomalous fields should not be at least as useful as vertical field TFs. Since anomalous horizontal fields at a site are mostly due to resistivity variations beneath a site, while vertical fields are more sensitive to structure off to the side, joint interpretation of both sorts of TFs (along with MT) should provide improved resolution. With widely spaced sites the value added by horizontal field TFs could be considerable. Note also that vertical field TFs can sometimes be severely affected by structures well outside the area being modeled, making these TFs difficult to fit. This difficulty seems less likely to be a problem for horizontal field TFs, which are less sensitive to distant structures. Inversion programs could easily be modified to allow interpretation of this additional information; it is time for code developers to do so.

The last area of application is the most in need of research, and offers the greatest possibility for significant advance. Interpretation strategies for EM induction data have long been constrained by limitations in data availability and limitations in modeling and inversion methods. Advances in both areas present us with much richer data sets, and with the potential to interpret them properly. This includes acknowledging (where appropriate) that the external sources are not necessarily as simple as we would like (and were previously forced to assume to make interpretation tractable). Extension of the classical HSG method to allow for quantitative two and three dimensional interpretation of gradient sources is a problem that is ripe for attack. Possibly this may allow for better control over large scale surface distortion, and thus significantly improved constraints on large scale upper mantle conductivity in widely spaced MT arrays.

Finally, in addition to the three areas of application emphasized here, arrays are of course the only way that we can really gain an understanding of the external sources. Although in many cases the details of these sources may be unimportant to researchers in induction, a thorough understanding of the external sources is likely to remain an important component in further advances in induction methods.

References

Alabi, A.O.: 1983, Magnetometer array studies, *Geophys. Surv.* **6**, 153–172.

Amm, O. and Viljanen, A.: 1998, Ionospheric disturbance magnetic field continuation from the ground to the ionosphere using spherical elementary current systems, *Earth Planets Space* **51**, 431–440.

Arora, B.R., Rigoti, A., Vitorello, I., Padilha, A.L., Trivedi, N.B., and Chamalaun, F.H.: 1998, Magnetometer array study in north-northeast Brazil: conductive image building and functional induction modes, *Pure Appl. Geophys.* **152**, 349–375.

Arora, B.R., Padilha, A.L., Vitorello, I., Trivedi, N.B., Fontes, S., Rigoti, A., and Chamalaun, F.H.: 1999, 2-D geoelectrical model for the Parnaiba basin conductivity anomaly, north-northeast Brazil and its tectonic implications, *Tectonocphysics* **302**, 57–69.

Bahr, K. and Filloux, J.H.: 1989, Local *Sq* responses from EMSLAB data, *Journal of Geophysical Research* **95**, 14,195–14,200.

Bailey, R.C., Edwards, R.N., Garland, G.D., Kurtz, R., and Pitcher, D.: 1974, Electrical conductivity studies over a tectonically active area in eastern Canada, *J. Geomagn. Geoelectr.* **26**, 125–146.

Banks, R.J.: 1969, Geomagnetic variations and the electrical conductivity of the upper mantle, *Geophys. J. Roy. Astr. Soc.* **17**, 457–487.

Banks, R.J.: 1986, The interpretation of the Northumberland Trough geomagnetic variation anomaly using two-dimensional current models, *Geophys. J. Roy. astr. Soc.* **79**, 595–616.

Banks, R.J., and Ainsworth, J.N.: 1992, Global induction and the spatial structure of mid-latitude geomagnetic variations, *Geophys. J. Int.* **110**, 251–266.

Banks, R.J., Irving, A.A.K., and Livelybrooks, D.W.: 1993, The simulation of magnetic variation anomalies using single station data, *Phys. Earth Planet. Inter.* **81**, 85–98.

Bannister, J.R. and Gough, D.I.: 1978, A study of two polar magnetic substorms with a two-dimensional magnetometer array, *Geophys. J. R. Astr. Soc.* **53**, 1–26.

Beamish D. and Johnson, P.M.: 1982, Difficulties in the application of magnetic field gradient analysis to induction studies in England, *Phys. Earth Planet. Int.* **28**, 1–13.

Beamish, D. and Banks, R.J.: 1983, Geomagnetic variation anomalies in Northern England: Processing and presentation of data from a non-simultaneous array, *Geophys. J. R. Astron. Soc.* **75**, 513–539.

Blackwell, D.B., Bowen, R.G., Hull, D.A., Riccio, J., and Steele, J.L.: 1982, Heat flow, arc volcanism and subduction in Northern Oregon, *J. Geophys. Res.* **87**, 8735–8754.

Blackwell, J.L. Steele, and Kelley, S.A.: 1985, Heat flow and geothermal studies in the State of Washington, *Open File Rep. 85-6*, Div. of Geol. and Earth Resour., Washington Dep. of Nat. Resour., Olympia.

Cerv, V., Pek, J., and Praus, O.: 1997, The present state of art of long period magnetotellurics in the western part of the Bohemian Massif, *J. Geomag. Geoelec.* **49**, 1559–1583.

Chamalaun, F.H. and Barton, C.E.: 1993, Electromagnetic induction in the Australian crust: results from the Australia-Wide Array of Geomagnetic Stations, *Explor. Geophys.* **24**, 179–186.

Chamalaun, F.H., Lilley, F.E.M., and Wang, L.J.: 1999, Mapping the Carpenteria conductivity anomaly in Northern Australia, *Phys. Earth. Planet. Int.* **116**, 105–115.

Chave, A.D., Thomson, D.J., and Ander, M.E.: 1987, On the robust estimation of power spectra, coherences, and transfer functions, *J. Geophys. Res.* **92**, 633–648.

Chave, A.D. and Thomson, D.J.: 1989, Some comments on magnetotelluric response function estimation, *J. Geophys. Res.* **94**, 14,215–14,226.

Chave, A.D. and Smith, J.T.: 1994, On electric and galvanic distortion tensor decomposition, *J. Geophys. Res.* **99**, 4669–4662.

Chen, L. and Hasegawa, A.: 1974, A theory of long-period geomagnetic pulsations, *Jour. Geophys. Res.* **79**, 1024–1032.

Chen, L., Booker, J.R., Jones, A.G., Wu, N., Unsworth, M., Wei, W., and Tan, H.: 1997, Electrically conductive crust in southern Tibet from INDEPTH magnetotelluric surveying, *Science* **274**, 1684–1688.

Chi, P.J. and Russell, C.T.: 1998, An interpretation of the cross-phase spectrum of geomagnetic pulsations by the file line resonance theory, *Geophyscal Research Letters* **25**, 4445–4448.

Dmitriev, V.I. and Berdichevsky, M.N.: 1979, The fundamental model of magnetotelluric sounding, *Proc. IEEE* **67**, 1033–1044.

Egbert, G.D.: 1989a, Multivariate analysis of geomagnetic array data II, Random source models, *J. Geophys. Res.* **94**, 14,229–14,267.

Egbert, G.D., 1989b, Multivariate splines for interpolation and separation of magnetometer array data, paper presented at: Sixth Scientific Assembly, Int. Assoc. Geomagn. Aeron., Exeter, England, 24 July–4 Aug.

Egbert, G.D.: 1991, On the synthesis of a large geomagnetic array from small overlapping arrays, *Geophys. J. Int.* **106**, 37–51.

Egbert, G.D.: 1997, Robust multiple station magnetotelluric data processing, *Geophys. J. Int.* **130**, 475–496.

Egbert, G. and Booker, J.R.: 1986, Robust estimation of geomagnetic transfer functions, *Geophys. J. R. Astron. Soc.* **87**, 173–194.

Egbert, G.D. and Booker, J.R.: 1989, Multivariate analysis of geomagnetic array data 1, The response space, *J. Geophys. Res.* **94**, 14,227–14,248.

Egbert, G.D. and Booker, J.R.: 1993, Imaging crustal structure in Southwestern Washington with small magnetometer arrays, *J. Geophys. Res.* **98**, 15,967–15,985.

Egbert, G.D., Eisel M., Boyd, O.S., and Morrison, H.F.: 2000, DC trains and Pc3s: source effects in mid-latitude geomagnetic transfer functions, *Geophys. Res. Lett.* **27**, 25–28.

Eisel, M. and Egbert, G.D.: 2001, On the stability of magnetotelluric transfer function estimates and the reliability of their variances, *Geophys. Jour. Int.* **144**, 65–82.

Ernst, T., Sokolova, E.Yu., Varentsov, Iv.M., and Golubev, N.G.: 2001, Comparison of two techniques for MT data processing using synthetic data sets, *Acta Geoph. Pol.* **49**, 213–243.

Frazer, M.C.: 1974, Geomagnetic deep sounding with arrays of magnetometers, *Rev. Geophys. Space Phys.* **12**, 401–420.

Fujinawa, Y., Honkura, Y., Kawakami, N., Asch, T.H., and Uyeshima, M.: 1997, Studies of the georesistivity structure in the central part of the northeastern Japan Arc, *J. Geomg. Geoelec.* **49**.

Gamble, T.D., Goubau, W.M., and Clarke, J.: 1979a, Magnetotellurics with a remote reference, *Geophysics* **44**, 53–68.

Gamble, T.D., Goubau, W.M., and Clarke, J.: 1979b, Error analysis for remote reference magnetotellurics, *Geophysics* **44**, 959–968.

Garcia, X., Chave, A.D., and Jones, A.G.: 1997, Robust processing of magnetotelluric data from the auroral zone, *J. Geomagn. Geoelectr.* **48**, 1451–1468.

Gough, D.I.: 1973, The interpretation of magnetometer array studies, *Geophys. J. R. Astr. Soc.*, **35**, 83–98.

Gough, D.I.:1986, Mantle upflow tectonics in the Canadian Cordillera, *J. Geophys. Res.* **91**, 1909–1919.

Gough, D.I.: 1989, Magnetometer array studies, earth structure, and tectonic processes, *Rev. Geophys.* **27**, 141–157.

Gough, D.I. and Reitzel, J.S.: 1967, A portable three-component magnetic variometer, *J. Geomag. Geoelec.* **19**, 203–215.

Gough, D.I. and Ingham, M.R.: 1983, Interpretation methods for magnetometer arrays, *Rev. Geophys. Space Phys.* **21**, 805–827.

Gough, D.I., McKirdy, D.M., Woods, D.V., and Geiger, H.: 1989, Conductive structures and tectonics beneath the EMSLAB land array, *J. Geophys. Res.* **94**, 14,099–14,110.

Huber, P.J.: 1981, *Robust Statistics*, Wiley, New York.

Jones, A.G.: 1980, Geomagnetic induction studies in Scandinavia – I. Determination of the inductive response function from the magnetometer data, *J. Geophys.* **48**, 181–194.

Jones, A.G. and Craven: 1990, The North American central plains conductivity anomaly and its correlation with gravity, magnetic, seismic, and heat flow data in Saskatchewan, Canada, *Phys. Earth Planet. Inter.* **60**, 169–194.

Korja, T. and BEAR Working Group: 2000, Baltic Electromagnetic Array Research: an overview, paper presented at 15th workshop on electromagnetic induction in the earth, Cabo Frio, Brazil, Aug. 19–26.

Kuckes, A.F.: 1973a, Relation between electrical conductivity of a mantle and fluctuating magnetic fields, *Geophys. J. R. Astr. Soc.* **32**, 119–131.

Kuckes, A.F.: 1973b, Correspondence between the magnetotelluric and field penetration analysis for measuring electrical conductivity, *Geophys. J. R. Astr. Soc.* **32**, 381–385.

Kuckes, A.F., Nekut, A.G., and Thompson, B.G.: 1985, A geomagnetic scattering theory for evaluation of earth structure, *Geophys. J. R. Astr. Soc.* **83**, 319–330.

Küppers, F., Untiedt, J., Baumjohann, W., Lange, K., and Jones, A.G.: 1979, A two-dimensional magnetometer array for ground-based observations of auroral zone electric currents during the International Magnetospheric Study (IMS), *J. Geophys.* **46**, 429–450.

Law, L.K., Auld, D.R., and Booker, J.R.: 1980, A geomagnetic variation anomaly coincident with the Cascade volcanic belt, *J. Geophys. Res.* **85**, 5297–5302.

Larsen, J.C., Mackie, R.L., Manzella, A., Fiordelisi, A., and Rieven, S.: 1996, Robust smooth magnetotelluric transfer functions, *Geophys. J. Int.* **124**, 801–819.

Lilley, F.E.M., Woods, D.V., and Sloane, M.N.: 1976, Electrical conductivity from Australian magnetometer arrays using spatial gradient data, *Phys. E. Pl. Int.*, **25**, 202–209.

Mackie, R.L. and Madden T.R.: A magnetotelluric survey around the Loma Prieta fault zone, *EOS, Trans. Am. Geophys. Un.* **73**, 99, 1992.

Olsen, N.: 1992, Day-to-day C-response estimation for S_q from 1 cpd to 6 cpd using the $Z : Y$ method, *J. Geomag. Geoelctr.* **44**, 433–447.

Olsen, N.: 1998, The electrical conductivity of the mantle beneath Europe derived from C-responses from 3 to 720 hr, *Geophys. J. Int.* **133**, 298–308.

Porath, H., Oldenburg, D.W., and Gough, D.I.: 1970, Separation of magnetic variation fields and conductive structure in the Western United States, *Geophys. J. R. Astr. Soc.* **19**, 237–260.

Richmond, A.D. and Baumjohann, W.: 1983, Three-dimensional analysis of magnetometer array data, *J. Geophys.* **54**, 138–156.

Ritter, O., Junge, A., and Dawes, G.J.K.: 1998, New equipment and processing for magnetotelluric remote reference observations *Geophys. J. Int.* **132**, 535–548.

Ritter, P. and Banks, R.J.: 1998, Separation of local and regional information in distorted GDS response functions by hypothetical event analysis, *Geophys. J. Int.* **135**, 923–942.

Rokityansky, I.I.: 1982, *Geoelectromagnetic Investigation of the Earth's Crust and Mantle*, New York: Springer-Verlag, 381 pp.

Schmucker, U.: 1970, Anomalies of geomagnetic variations in the Southwestern United States, *Bull. Scripps Inst. Oceanogr.* **13**.

Schultz, A. and Larsen, J.C.: 1987, On the electrical conductivity of the Earth's interior I: mid-mantle response function computation, *Geophys. J. Roy. Astr. Soc.* **88**, 763–781.

Sims, W.E., Bostick, F.X., and Smith, H.W.: 1971, The estimation of magntotelluric impedance tensor elements from measured data, *Geophysics* **36**, 938–942.

Sokolova, E., Varentsov, I., and the BEAR Working Group: 2001, Investigation and elimination of polar magnetotelluric source distortions in the BEAR project transfer functions, submitted to *Earth, Planets, Space*.

Soyer, W. and Brasse, H.: 2001, Investigation of anomalous magnetic field variations in the central Andes of N Chile and SW Bolivia submitted to *Geophys. Res. Lett.*

Stanley, W.D.: 1984, Tectonic study of Cascade Range and Columbia Plateau in Washington State based on magnetotelluric soundings, *J. Geophys. Res.* **89**, 4447–4460.

Unsworth M.J., Malin, P.E., Egbert, G.D., and Booker, J.R.: 1997, Internal structure of the San Andreas fault at Parkfield, California, Geology**25**, 359–362.

Unsworth, M., Bedrosian, P., Eisel, M., Egbert, G., and Siripunvaraporn, W.: 2000, Along strike variations in the electrical structure of the San Andreas Fault at Parkfield, California, *Geophys. Res. Lett.* **27**, 3021–3024.

Varentsov, Iv.M., Sokolova, E.Yu., Martanus, E.R., Nalivaiko, K.V., and the BEAR working group: 2001, Robust procedures to estimate transfer functions in the Baltic electromagnetic array research (BEAR), submitted to *Earth, Planets, Space*.

Viljanen, A., Amm, O., Pulkkinen, A., and the BEAR Working Group: 2000, Magnetic field separation: use of a two-dimensional magnetometer array with some improvements of the field

interpolation, paper presented at 15th workshop on electromagnetic induction in the earth, Cabo Frio, Brazil, Aug. 19–26.

Wang, L.J. and Lilley, F.E.M.: 1999, Inversion of magnetometer array data by thin sheet modeling, Geophys. J. Int. **137**, 128–138.

Wannamaker, P.E., Booker, J.R., Jones, A.G., Chave, A.D., Filloux, J.H., Waff, H.S., and Law, L.K.: 1989, Resistivity cross-section through the Juan de Fuca subduction system and its tectonic implications, *J. Geophys. Res.* **94**, 14,127–14,145.

Waters, C.L., Menk, F.W., and Fraser, B.J.: 1991, The resonance structure of low latitude Pc3 geomagnetic pulsations, *Geophyscal Research Letters* **18**, 2293–2296.

Zhdanov, M.S., Traynin P., and Booker, J.R.: 1996, Underground imaging by frequency domain electromagnetic migration, *Geophysics* **61**, 666–682.